PASSIVE SUPPRESSION OF HELICOPTER GROUND RESONANCE INSTABILITY BY MEANS OF A STRONGLY NONLINEAR ABSORBER

Baptiste Bergeot, Sergio Bellizzi, B Cochelin

PASSIVE SUPPRESSION OF HELICOPTER GROUND RESONANCE INSTABILITY BY MEANS OF A STRONGLY NONLINEAR ABSORBER

B. Bergeot[1*], S. Bellizzi[1] and B. Cochelin[1]

[1]LMA, CNRS, UPR 7051, Centrale Marseille, Aix-Marseille Univ, F-13420 Marseille Cedex 20, France
*Corresponding author: baptiste.bergeot@centrale-marseille.fr

NOise and VIbration - EMerging Technologies, NOVEM2015
April 13-15 2015, Dubrovnik - Croatia

Abstract

In this paper, we study a problem of passive suppression of helicopter Ground Resonance (GR) using a single degree freedom Nonlinear Energy Sink (NES). GR is a dynamic instability involving the coupling of the blades motion in the rotational plane (i.e. the lag motion) and the helicopter fuselage motion. A reduced linear system reproducing GR instability is used. It is obtained using successively Coleman transformation and binormal transformation. The analysis of the steady-state responses of this model is performed when a NES is attached on the helicopter fuselage. The NES includes linear damping and essential cubic restoring force. The analysis is achieved applying complexification-averaging method and slow-fast partition of the motion. The resulting slow-flow model is finally analyzed using multiple scale approach. Four steady-state responses are highlighted and explained theoretically: complete suppression, partial suppression through strongly modulated response, partial suppression through periodic response and no suppression of the GR. An algorithm based on simple criterions is developed to predict these steady-state response regimes. Numerical simulations of the complete system confirm this analysis of the slow-flow dynamics. A parametric analysis of the influence of the NES damping coefficient and the rotor speed on the response regime is finally proposed.

1 Introcuction

Ground Resonance (GR) is a potential destructive mechanical instability that occurs in helicopters, generally when the aircraft is on the ground. The phenomenon of GR involves a coupling between the airframe motion on its landing gear and the blades motion in the rotational plane (i.e. the lag motion). It can be investigated without taking into account the aerodynamical effects. The standard reference of the GR analysis is the paper by Coleman and Feingold [4] where it is established, considering an isotropic rotor, that GR is due to a frequency coalescence between a lag mode and the fuselage mode. The range of rotors speeds Ω for which this frequency coalescence occurs is predicted analytically. More references can be found in [2, 10], a recent analysis of helicopter GR with asymmetric blades is proposed in [18]. Traditionally, GR instability is prevented by two passive methods: increasing the damping [5] or modify the stiffness of the rotor blade lag mode or the fuselage mode. Active control of GR has been also studied [10].

Targeted Energy Transfer (TET) is a concept based on an additional essentially nonlinear attachment also named Nonlinear Energy Sink (NES) to an existing primary linear system. TET has been extensively studied numerically, theoretically and expermentally, the results prove that the NES is very efficient for vibration mitigation [22] and noise reduction [1]. Impulsive loading was theoretically analyzed for example in [21] where TET is investigated in terms of resonance capture. In [20], harmonic forcing was considered where response regimes are characterized in terms of periodic and strongly modulated responses using an asymptotic analysis (multi scale approach) of the averaged flow obtained using the complexification-averaging method [16].

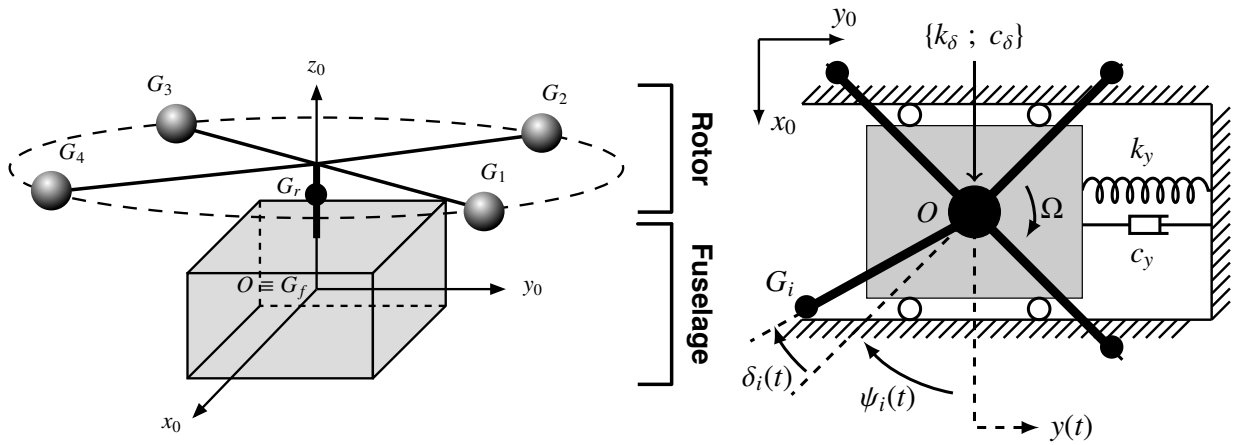

Figure 1: Descriptive diagram of the used helicopter system. (a) Overview of the system. (b) View from the top.

NESs are also used to control dynamic instabilities. The possible suppression of the limit cycle oscillations of a Van der Pol oscillator utilizing a NES is demonstrated numerically in [11] and studied theoretically in [6]. A series of papers [12, 13, 7] demonstrated that a NES coupled to a rigid wing in subsonic flow can partially or even completely suppress aeroelastic instability. In [12], the suppression mechanisms are investigated numerically. Several aspects of the suppression mechanisms are validated expermentally in [13]. Finally an asymptotic analysis is reported in [7] demonstrating the existence of the three passive suppression mechanisms based on TET. Suppression of aeroelastic instability of a general nonlinear multi degree of freedom system has also be considered in [15].

In this context, the use of a NES appears to be an interesting alternative way to control GR instability. Indeed, the only possible effect of using linear dampers is to suppress completely (or not at all) the instability and the adding damping needed for the suppression may be very large. For its part, a NES attachment with a relatively small linear damping and a pure nonlinear stiffness, is able to prevent destructive amplitude of oscillations even if GR instability persists. This situations are hereafter referred as *partial suppression mechanisms*. The goal of the paper is therefore to study the effect of attaching a NES on the fuselage, in ungrounded configuration, on the helicopter GR instability. We focus on the characterization of the steady-state response regimes of a helicopter ground resonance model including a ungrounded NES attachment.

The paper is organized as follows. In Sect. 2, firstly, the simplest helicopter model reproducing GR phenomenon is presented. It involves only lag motion of the four blades and one direction of the fuselage motion. Then, a NES is attached to the fuselage in an ungrounded configuration leading to the Simplest Helicopter Model including a NES (hereafter referred as SHM+NES). The Sect. 3 first presents some the steady-state response regimes which result from the NES attachment. We count four regimes classified into two categories depending on the fact that the trivial solution of the SHM+NES is stable or not. Then, an analytical procedure based on complexification-averaging method together with multiple scale approach [17] is developed to analyze situations for which trivial solution of the SHM+NES is unstable. Moreover, a systematic procedure for the prediction of the steady-state response regimes is presented. In Sect. 4, the procedure is used to analyze the influence of the damping of the NES and the rotor speed on the response regimes. Finally numerical validation of the method is performed.

2 The Simplest Helicopter Model including a Non Linear Energy Sink (SHM+NES)

2.1 Simplest Helicopter Model (SHM) that can describe ground resonance

To carry out the analytical approach presented in this work (in Sect. 3) we need to obtain a helicopter model with a smaller number of Degrees Of Freedom (DOF). For that, a reference helicopter model, with

10 DOF in state-space, is simplified using successively Coleman transformation [4] and binormal transformation [5] leading to the SHM which has 4 DOF in state-space.

The reference model is very similar to that described for example in [9, 2, 10]. Here, it describes an idealized helicopter which consists of a fuselage on which a 4-blades rotor rotates at a constant speed Ω. Moreover, only lag motions are taken into account. To obtain the equations of motion a earth-fixed system of coordinates (O, x_0, y_0, z_0) is considered where the origin O coincides with the center of inertia G_f of the fuselage at rest (see Fig. 1). At rest, the center of inertia of the rotor G_r is also located on the axis (O, z_0). The fuselage is a simple damped mass-spring system with only one translational DOF $y(t)$. Blades, which are assumed to be a mass points G_i (with $i \in [1, 4]$) placed at a distance L from the axis (O, z_0), are described by the lagging angles $\delta_i(t)$. A lagging angle is the angle between the current position of the blade and its equilibrium position $\xi_i(t) = \Omega t - \frac{\pi}{2}(i-1)$ (see Fig. 1(b)). The equations of motion which govern the time evolution of the five DOFs of the model (the fuselage displacement $y(t)$ and the four lagging angles $\delta_i(t)$) are derived using Lagrange method. This leads to the reference model

$$\begin{cases} (m_y + 4m_\delta)\,\ddot{y} + c_y\dot{y} + k_y y \; + \\ M_\delta \sum_{j=1}^{4} \left\{ \ddot{\delta}_j \cos(\xi_j + \delta_j) - \left(\Omega + \dot{\delta}_j\right)^2 \sin(\xi_j + \delta_j) \right\} = 0 & \text{(1a)} \\ I_\delta \ddot{\delta}_i + c_\delta \dot{\delta}_i + k_\delta \delta_i + M_\delta \ddot{y} \cos(\xi_i + \delta_i) = 0, \; i = 1, 4 & \text{(1b)} \end{cases}$$

where " $\dot{}$ " denotes the derivative with respect to time t, m_y is the fuselage mass, m_δ is the mass of a blade, $M_\delta = m_\delta L$ and $I_\delta = m_\delta L^2$ are the static moment and the moment of inertia of one blade respectively, c_y, c_δ are damping coefficients of the the fuselage and of a blade respectively and k_y and k_δ are linear stiffness coefficients.

After linearization of the reference model (1) around the trivial equilibrium point, a change of variables which transforms individual motions of the blades (described by the lagging angles) into collective motions described by the so-called Coleman coordinates [4] is applied. For a 4-blades rotor there are four Coleman coordinates δ_0, δ_{1c}, δ_{1s} and δ_{cp} defined by

$$\delta_0(t) = \frac{1}{4}\sum_{j=1}^{4} \delta_j(t), \qquad \delta_{1c}(t) = \frac{1}{2}\sum_{j=1}^{4} \delta_j(t)\cos(\xi_j(t)), \tag{2}$$

$$\delta_{1s}(t) = \frac{1}{2}\sum_{j=1}^{4} \delta_j(t)\sin(\xi_j(t)), \qquad \delta_{cp}(t) = \frac{1}{4}\sum_{j=1}^{4} (-1)^j \delta_j(t). \tag{3}$$

One can be shown that the variables δ_0 and δ_{cp} are uncoupled and can be discarded. The reason of the decoupling is the fact that the collective motions δ_0 and δ_{cp} leave the rotor center of inertia motionless. As a result, a system of equations with three DOF, namely y, δ_{1c} and δ_{1s}, is obtained.

Introducing the following notations

$$\begin{array}{ll} \omega_y^2 = k_y/\left(m_y + 4m_\delta\right), & \omega_\delta^2 = k_\delta/I_\delta; \\ \tilde{\lambda}_y = c_y/\left(m_y + 4m_\delta\right), & \tilde{\lambda}_\delta = c_\delta/I_\delta \\ \tilde{S}_d = 2M_\delta/\left(m_y + 4m_\delta\right), & \tilde{S}_c = M_\delta/I_\delta = 1/L. \end{array} \tag{4}$$

where ω_y and ω_δ are the natural frequency of the fuselage and of one blade respectively and $\tilde{S}_c$ and $\tilde{S}_d$ are the coupling coefficients, equations of motion are finally written in matrix form

$$\mathbf{M}\ddot{\mathbf{X}} + (\mathbf{C} + \mathbf{G})\dot{\mathbf{X}} + \mathbf{K}\mathbf{X} = \mathbf{0}, \qquad \text{with} \qquad \mathbf{X} = [\mathbf{y}\ \delta_{\mathbf{1c}}\ \delta_{\mathbf{1s}}]^{\mathbf{t}}. \tag{5}$$

$\mathbf{M}$, $\mathbf{K}$, $\mathbf{C}$ and $\mathbf{G}$, are mass matrix, stiffness matrix, damping matrix and gyroscopic matrix of the system respectively, they are defined by

$$\mathbf{M} = \begin{bmatrix} 1 & \tilde{S}_d & 0 \\ \tilde{S}_c & 1 & 0 \\ 0 & 0 & 1 \end{bmatrix}, \qquad \mathbf{K} = \begin{bmatrix} \omega_y^2 & 0 & 0 \\ 0 & \omega_\delta^2 - \Omega^2 & \tilde{\lambda}_\delta \Omega \\ 0 & -\tilde{\lambda}_\delta \Omega & \omega_\delta^2 - \Omega^2 \end{bmatrix}, \tag{6}$$

$$\mathbf{C} = \begin{bmatrix} \tilde{\lambda}_y & 0 & 0 \\ 0 & \tilde{\lambda}_\delta & 0 \\ 0 & 0 & \tilde{\lambda}_\delta \end{bmatrix}, \qquad \mathbf{G} = \begin{bmatrix} 0 & 0 & 0 \\ 0 & 0 & 2\Omega \\ 0 & -2\Omega & 0 \end{bmatrix}. \tag{7}$$

Note that $\tilde{S}_d$ and $\tilde{S}_c$ characterize the fuselage/rotor coupling.

Helicopter ground resonance. The phenomenon is explained making a stability analysis of the previous linear system (5). The set of eigenvalues α_i (with $i \in [1, 6]$) are easily computed from $\mathbf{M}$, $\mathbf{K}$, $\mathbf{C}$ and $\mathbf{G}$. Note that if the fuselage/rotor coupling is suppressed (i.e. stating $\tilde{S}_c = \tilde{S}_d = 0$), the eigenvalues of the system correspond to the natural eigenvalues of the fuselage, denoted $\alpha_{f,i}$ (with $i \in [1, 2]$), and of the rotor, denoted $\alpha_{r,i}$ (with $i \in [1, 4]$). In Fig. 2(a), the typical behavior of the imaginary part of these eigenvalues is reported with respect to the rotor speed Ω for $\omega_y < \omega_\delta$. We can notice that there are two values of Ω for which an interaction between the fuselage mode and the regressive rotor mode is possible: $\Omega \approx |\omega_y - \omega_\delta|$ and $\Omega \approx \omega_y + \omega_\delta$[1].

In Figs. 2(b) and 2(c), the comparison between eigenvalues of the uncoupled systems $\alpha_{f,i}$ and $\alpha_{r,i}$ and the eigenvalues α_i of the coupled system shows that:

- For $\Omega \approx |\omega_y - \omega_\delta|$, a phenomenon of "curve veering" [14] appears, the real part of the eigenvalues α stay negative and there is no instability.
- For $\Omega \approx \omega_y + \omega_\delta$, a phenomenon of frequency coalescence is observed, the real part of one of the eigenvalues α becomes positive and a dynamic instability occurs; this is the helicopter ground resonance.

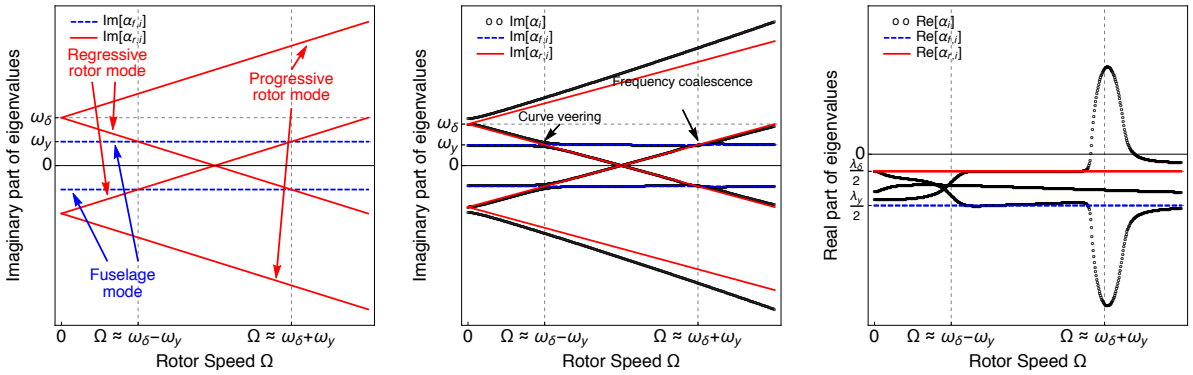

Figure 2: Eigenvalues of the uncoupled system and coupled system (5) for $\omega_y < \omega_\delta$. (a) Imaginary parts of the natural eigenvalues α_f of the fuselage (dashed blue line) and α_r of the rotor (solid red line). Comparison between the eigenvalues of the uncoupled systems (i.e. α_f and α_r) and the eigenvalues α of the coupled system (black circles): (b) imaginary parts and (c) real parts. Parameters used: $\omega_y = 1$, $\omega_\delta = 2$, $\tilde{\lambda}_y = 0.09$, $\tilde{\lambda}_\delta = 0.03$, $\tilde{S}_c = 0.6$ and $\tilde{S}_d = 0.3$. The parameters $\tilde{\lambda}_y$, $\tilde{\lambda}_\delta$, $\tilde{S}_c$ and $\tilde{S}_d$ are chosen to obtain readable figures, no for their realism.

Fig. 2 shows also that the progressive rotor mode does not interact with the fuselage mode. For $\omega_y > \omega_\delta$, similar observations can be made and consequently, in both situations ($\omega_y < \omega_\delta$ and $\omega_y > \omega_\delta$), the progressive rotor mode does not contribute to the creation of the GR instability. Therefore, the last step to obtain the

[1]If undamped system would be considered (i.e. if $\lambda_y = \lambda_\delta = 0$), we would get exact equalities: $\Omega = |\omega_y - \omega_\delta|$ and $\Omega = \omega_y + \omega_\delta$, see [9] for more details.

simplest model for helicopter ground resonance is to eliminate the progressive rotor mode from the equations of motion. This is achieved in the remaining of the section applying bi-normal transformation [3, 5] to the equations of motion of the rotor alone. In the state-space form we obtain

$$\dot{\mathbf{U}}_\mathbf{r} = \mathbf{A}_\mathbf{r}\mathbf{U}_\mathbf{r}, \qquad \text{with} \qquad \mathbf{U}_\mathbf{r} = \left[\delta_{1c}\ \delta_{1s}\ \dot{\delta}_{1c}\ \dot{\delta}_{1s}\right]^t. \tag{8}$$

The following eigenvalue problems:

$$\mathbf{A}_\mathbf{r}\mathbf{r} = \alpha_\mathbf{r}\mathbf{r} \quad \text{and} \quad \mathbf{A}_\mathbf{r}^\mathbf{t}\mathbf{l} = \alpha_\mathbf{r}\mathbf{l} \tag{9}$$

where $\mathbf{A}_\mathbf{r}^\mathbf{t}$ denotes the transpose of $\mathbf{A}_\mathbf{r}$, are solved giving:

- two pairs of complex conjugates eigenvalues: $\alpha_{r,1}$, $\alpha_{r,1}^*$, $\alpha_{r,2}$ and $\alpha_{r,2}^*$ (the " * " is the usual notation for the complex conjugate),
- two pairs of complex conjugates eigenvectors of $\mathbf{A}_\mathbf{r}$, $\mathbf{r_i}$, called *right eigenvectors* of $\mathbf{A}_\mathbf{r}$: $\mathbf{r_1}$, $\mathbf{r_1^*}$, $\mathbf{r_2}$ and $\mathbf{r_2^*}$.
- two pairs of complex conjugates eigenvectors of $\mathbf{A}_\mathbf{r}^\mathbf{t}$, $\mathbf{l_i}$, called *left eigenvectors* of $\mathbf{A}_\mathbf{r}$: $\mathbf{l_1}$, $\mathbf{l_1^*}$, $\mathbf{l_2}$ and $\mathbf{l_2^*}$.

The right and left eigenvectors satisfy the biorthogonality properties: $\mathbf{L}^\mathbf{t}\mathbf{R}$ and $\mathbf{L}^\mathbf{t}\mathbf{A}_\mathbf{r}\mathbf{R}$ are diagonal matrices where $\mathbf{R} = [\mathbf{r_1}\ \mathbf{r_1^*}\ \mathbf{r_2}\ \mathbf{r_2^*}]$ and $\mathbf{L} = [\mathbf{l_1}\ \mathbf{l_1^*}\ \mathbf{l_2}\ \mathbf{l_2^*}]$. It is convenient to normalize the two set of eigenvectors $\mathbf{r_i}$ and $\mathbf{l_i}$ in order to obtain

$$\mathbf{L}^\mathbf{t}\mathbf{R} = \mathbf{I}. \tag{10}$$

In this case, we have:

$$\mathbf{L}^\mathbf{t}\mathbf{A}_\mathbf{r}\mathbf{R} = \begin{bmatrix} \alpha_{r,1} & 0 & 0 & 0 \\ 0 & \alpha_{r,1^*} & 0 & 0 \\ 0 & 0 & \alpha_{r,2} & 0 \\ 0 & 0 & 0 & \alpha_{r,2^*} \end{bmatrix} = \mathbf{D}_\mathbf{r}. \tag{11}$$

The binormal transformation consists in introducing the binormal coordinates which are constituted of two pairs of complex conjugates, (q_1, q_1^*) and (q_2, q_2^*), and defined by the following relation

$$\mathbf{U}_\mathbf{r} = \mathbf{R}\mathbf{Q} \ \Leftrightarrow\ \mathbf{Q} = \mathbf{L}^\mathbf{t}\mathbf{U}_\mathbf{r}, \quad \text{with} \quad \mathbf{Q} = [q_1\ q_1^*\ q_2\ q_2^*]^t. \tag{12}$$

Introducing Eq. (12) in Eq. (8), the equations of motion of the rotor take the form of the following diagonal system

$$\dot{\mathbf{Q}} = \mathbf{D}_\mathbf{r}\mathbf{Q}. \tag{13}$$

One of the couples (q_1, q_1^*) and (q_2, q_2^*) is relative to the progressive rotor mode and the other the regressive one. The couple (q_2, q_2^*) is arbitrary chosen to be relative to the progressive rotor mode and since this mode does not destabilize the system, the variables q_2 and q_2^* can be removed from the analysis.

Consequently, using the vector $\mathbf{U}_\mathbf{r}$, equations of motion of the whole coupled system, i.e. Eqs (5), become

$$\begin{cases} \ddot{y} + \tilde{\lambda}_y\dot{y} + \omega_y^2 y + \tilde{S}_d\dot{\mathbf{U}}_{\mathbf{r},3} = 0 & \text{(14a)} \\ \dot{\mathbf{U}}_\mathbf{r} = \mathbf{A}_\mathbf{r}\mathbf{U}_\mathbf{r} + \begin{bmatrix} 0 \\ 0 \\ \tilde{S}_c\ddot{y} \\ 0 \end{bmatrix}. & \text{(14b)} \end{cases}$$

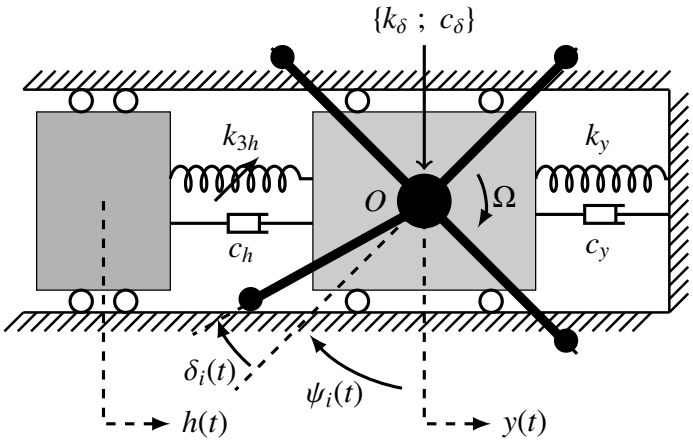

Figure 3: Descriptive diagram of the used helicopter system coupled to an ungrounded NES. View from the top.

Then using Eq. (13) (ignoring variables q_2 and q_2^*) and the following relations

$$\alpha_{r,2} = \alpha^*_{r,1}, \qquad \mathbf{R}_{32} = \mathbf{R}^*_{31}, \qquad \mathbf{L}_{32} = \mathbf{L}^*_{31}, \tag{15}$$

Eqs. (14) become finally

$$\begin{cases} \ddot{y} + \tilde{\lambda}_y \dot{y} + \omega_y^2 y + \tilde{S}_d \left(\mathbf{R}_{31}\dot{q}_1 + \mathbf{R}^*_{31}\dot{q}^*_1\right) = 0 & \text{(16a)} \\ \dot{q}_1 - \alpha_{r,1} q_1 + \tilde{S}_c \mathbf{L}_{31} \ddot{y} = 0. & \text{(16b)} \end{cases}$$

Eqs. (16) define the Simplest Helicopter Model (the SHM with 4 DOF in state-space) that can describe GR phenomenon.

2.2 The Simplest Helicopter Model including a Non Linear Energy Sink (SHM+NES)

The simplified model (16) is used to study the effect of attaching a NES on the fuselage of the helicopter. For that, a NES with a mass m_h, a damping coefficient c_h and a cubic stiffness k_{3h}, is attached on the fuselage in an ungrounded configuration (see Fig. 3). Taking into account the NES displacement $h(t)$, the equations of motion read

$$\begin{cases} \ddot{y} + \tilde{\lambda}_y \dot{y} + \omega_y^2 y + \tilde{S}_d \left(\mathbf{R}_{31}\dot{q}_1 + \mathbf{R}^*_{31}\dot{q}^*_1\right) + \tilde{\mu}\left(\dot{y} - \dot{h}\right) + \tilde{\alpha}_3 \left(y - h\right)^3 = 0 & \text{(17a)} \\ \epsilon \ddot{h} + \tilde{\mu}\left(\dot{h} - \dot{y}\right) + \tilde{\alpha}_3 \left(h - y\right)^3 = 0 & \text{(17b)} \\ \dot{q}_1 - \alpha_{r,1} q_1 + \tilde{S}_c \mathbf{L}_{31} \ddot{y} = 0, & \text{(17c)} \end{cases}$$

where $\epsilon = m_h / \left(m_y + 4m_\delta\right)$ is the mass ratio, $\tilde{\mu} = c_h / \left(m_y + 4m_\delta\right)$ and $\tilde{\alpha}_3 = k_{3h} / \left(m_y + 4m_\delta\right)$.

System of Eqs. (17) is the Simplest Helicopter Model including a Non Linear Energy Sink (SHM+NES).

2.2.1 Fixed points of the SHM+NES and their stability.

It is easy to show that the only fixed point of the SHM+NES (Eqs (17)) is the trivial solution $y = h = q_1 = 0$. To find its stability, the 6 eigenvalues of the Jacobian matrix of the state-space representation of the system Eqs (17) have to be computed. The trivial solution is unstable is one of the eigenvalues have positive real part.

3 Steady-state response regimes of the SHM+NES

3.1 Some steady-state response regimes

Using numerical integration of the SHM+NES, Eqs. (17), four different types of response regimes which may be highlighted (as illustrated in Sect. 4) when a NES is attached on the fuselage. They are classified into two categories depending on the fact that the trivial solution of the SHM+NES is stable or not:

- **The trivial solution of the SHM+NES is stable:**
  - *Complete suppression.* In this case, the additional damping due to the NES attachment stabilizes the system and the GR instability is completely suppressed.
- **The trivial solution of the SHM+NES is unstable**:
  - *Partial suppression through Periodic Response (PR).* In this case, the steady-state response regime is periodic with frequency close to ω_y[2].
  - *Partial suppression through Strongly Modulated Response (SMR).* In this case, the steady-state response regime is a quasiperiodic regime which exhibits a "fast" component with frequency close to ω_y and a "slow" component corresponding to the envelope of the signal. The term "Strongly modulated response" has been introduced by Starosvetsky and Gendelman [20] for the study of a forced linear system coupled to a NES.
  - *No suppression of GR.* The NES is not able to maintain stable steady-state regimes. We observe exponential growth of the fuselage displacement.

These four responses are also observed by Lee et al. [12] and study theoretically by Gendelman et al. [7] in the context of the control aeroelastic instabilities of a rigid wing in subsonic flow by means of a NES.

In the following sections an analytical procedure based on complexification-averaging method together with geometric singular perturbation theory is developed to analyze situations for which trivial solution of the SHM+NES is unstable.

3.2 The complexified-averaged model

The analytical study proposed is based on *complexification-averaging method* first introduced by Manevitch [16] and discussed in detail by Vakakis et al. [22].

First, to simplify the following calculations, it is convenient to introduce barycentric coordinates $v(t)$ and $w(t)$

$$v = y + \epsilon h \qquad \text{and} \qquad w = y - h. \tag{18}$$

Using Eqs. (18), Eqs. (17) are written as follow

$$\begin{cases} \ddot{v} + \tilde{\lambda}_y \dfrac{\dot{v} + \epsilon \dot{w}}{\epsilon + 1} + \omega_y^2 \dfrac{v + \epsilon w}{\epsilon + 1} + \tilde{S}_d \left(\mathbf{R}_{31} \dot{q}_1 + \mathbf{R}_{31}^* \dot{q}_1^* \right) = 0 & \text{(19a)} \\ \ddot{w} + \tilde{\lambda}_y \dfrac{\dot{v} + \epsilon \dot{w}}{\epsilon + 1} + \omega_y^2 \dfrac{v + \epsilon w}{\epsilon + 1} + \tilde{S}_d \left(\mathbf{R}_{31} \dot{q}_1 + \mathbf{R}_{31}^* \dot{q}_1^* \right) + \\ \qquad \tilde{\mu} \dfrac{1 + \epsilon}{\epsilon} \dot{w} + \tilde{\alpha}_3 \dfrac{1 + \epsilon}{\epsilon} w^3 = 0 & \text{(19b)} \\ \dot{q}_1 - \alpha_{r,1} q_1 + \tilde{S}_c \mathbf{L}_{31} \dfrac{\ddot{v} + \epsilon \ddot{w}}{\epsilon + 1} = 0. & \text{(19c)} \end{cases}$$

Secondly, the complexification[3] consists in introducing the following change of variable

[2] This can be shown for example by computing the power spectrum of the steady part of the signal.

[3] This step is not necessary for the variable $q_1(t)$ because it is already a complex variable.

$$\psi_1 = \dot{v} + j\omega_y v \qquad \text{and} \qquad \psi_2 = \dot{w} + j\omega_y w, \tag{20}$$

with $j^2 = -1$.

Previous numerical and theoretical results (see Sect. 3.1) motive us to introduce the assumption that the variable v, w and q_1 may be broken down into fast and slow components. For that, the following representation is introduced

$$\psi_1 = \phi_1 e^{j\omega_y t}\,, \qquad \psi_2 = \phi_2 e^{j\omega_y t}\,, \qquad q_1 = \phi_3 e^{j\omega_y t}, \tag{21}$$

where ϕ_i (with $i \in [1,3]$) is the complex slow modulated amplitude of the fast component $e^{j\omega_y t}$.

Substituting Eqs. (20) into Eqs. (19) an equivalent complex system of differential equations is obtained. Substituting next Eq. (21) in this complex system and performing an averaging over one period of the frequency ω_y yield to a system of equations describing the behavior of the slow complex amplitudes ϕ_i

$$\begin{cases} \dot{\phi}_1 + j\dfrac{\omega_y}{2}\phi_1 + \dfrac{\tilde{\lambda}_y - j\omega_y}{2(1+\epsilon)}\left(\phi_1 + \epsilon\phi_2\right) + \tilde{S}_d \mathbf{R}_{31}\left(\dot{\phi}_3 + j\omega_y\phi_3\right) = 0 & \text{(22a)} \\ \dot{\phi}_2 + j\dfrac{\omega_y}{2}\phi_2 + \dfrac{\tilde{\lambda}_y - j\omega_y}{2(1+\epsilon)}\left(\phi_1 + \epsilon\phi_2\right) + \tilde{S}_d \mathbf{R}_{31}\left(\dot{\phi}_3 + j\omega_y\phi_3\right) + \\ \qquad\qquad \dfrac{\tilde{\mu}}{2}\dfrac{1+\epsilon}{\epsilon}\phi_2 - j\dfrac{3\tilde{\alpha}_3}{8\omega_y^3}\dfrac{1+\epsilon}{\epsilon}\phi_2\left|\phi_2\right|^2 = 0 & \text{(22b)} \\ \dot{\phi}_3 + \left(j\omega_y - \alpha_{r,1}\right)\phi_3 + \dfrac{\tilde{S}_c}{1+\epsilon}\mathbf{L}_{31}\left[\left(\dot{\phi}_1 + \epsilon\dot{\phi}_2\right) + j\dfrac{\omega_y}{2}\left(\phi_1 + \epsilon\phi_2\right)\right] = 0. & \text{(22c)} \end{cases}$$

Eqs. (22) define the complexified-averaged system.

3.3 Approximation of the periodic solutions of the SHM+NES and their stability

The fixed point of the complexified-averaged system (22) (defined as $\dot{\phi}_i = 0$ for $i \in [1,3]$) only characterizes periodic solutions of Eqs. (19) if the frequency of the periodic solutions is equal to ω_y, the frequency used to defined the complex variables (20). However, using the polar coordinates $n_i(t)$ and $\theta_i(t)$ (with $i \in [1,3]$), defined by

$$\phi_i(t) = n_i(t)e^{j\theta_i(t)}, \tag{23}$$

and considering not the arguments $\theta_i(t)$ directly but the argument differences $\delta_{i1} = \theta_i(t) - \theta_1(t)$, the periodic solutions of the system of Eqs. (19) (and consequently of the SHM+NES (17)) may be defined from the complexified-averaged system (22) as the fixed points of the system of differential equations describing the dynamic of the variables n_1, n_2, n_3, δ_{21} and δ_{31}.

To obtain this system, Eqs. (22) are first re-written using matrix form

$$\dot{\mathbf{\Phi}} = \mathbf{C}\mathbf{\Phi} + \phi_2|\phi_2|^2\mathbf{H}, \tag{24}$$

where the constant complex matrices $\mathbf{C}$ and $\mathbf{H}$ are not specified (and easy obtained from Eqs. (22)).

Next introducing the polar coordinates (23) and separating real and imaginary parts of each equation,

Eq. (24) take the form

$$\begin{cases} \dot{n}_1 = n_1 \mathrm{Re}\left[\mathbf{C}_{11}\right] + n_2 \mathrm{Re}\left[\mathbf{C}_{12} e^{j\delta_{21}}\right] + n_3 \mathrm{Re}\left[\mathbf{C}_{13} e^{j\delta_{31}}\right] + n_2^3 \mathrm{Re}\left[\mathbf{H}_1 e^{j\delta_{21}}\right] & \text{(25a)} \\ n_1 \dot{\theta}_1 = n_1 \mathrm{Im}\left[\mathbf{C}_{11}\right] + n_2 \mathrm{Im}\left[\mathbf{C}_{12} e^{j\delta_{21}}\right] + n_3 \mathrm{Im}\left[\mathbf{C}_{13} e^{j\delta_{31}}\right] + n_2^3 \mathrm{Im}\left[\mathbf{H}_1 e^{j\delta_{21}}\right] & \text{(25b)} \\ \dot{n}_2 = n_1 \mathrm{Re}\left[\mathbf{C}_{21} e^{-j\delta_{21}}\right] + n_2 \mathrm{Re}\left[\mathbf{C}_{22}\right] + n_3 \mathrm{Re}\left[\mathbf{C}_{23} e^{j(\delta_{31}-\delta_{21})}\right] + n_2^3 \mathrm{Re}\left[\mathbf{H}_2\right] & \text{(25c)} \\ n_2 \dot{\theta}_2 = n_1 \mathrm{Im}\left[\mathbf{C}_{21} e^{-j\delta_{21}}\right] + n_2 \mathrm{Im}\left[\mathbf{C}_{22}\right] + n_3 \mathrm{Im}\left[\mathbf{C}_{23} e^{j(\delta_{31}-\delta_{21})}\right] + n_2^3 \mathrm{Im}\left[\mathbf{H}_2\right] & \text{(25d)} \\ \dot{n}_3 = n_1 \mathrm{Re}\left[\mathbf{C}_{31} e^{-j\delta_{31}}\right] + n_2 \mathrm{Re}\left[\mathbf{C}_{32} e^{j(\delta_{21}-\delta_{31})}\right] + n_3 \mathrm{Re}\left[\mathbf{C}_{33}\right] + n_2^3 \mathrm{Re}\left[\mathbf{H}_3 e^{j(\delta_{21}-\delta_{31})}\right] & \text{(25e)} \\ n_3 \dot{\theta}_3 = n_1 \mathrm{Im}\left[\mathbf{C}_{31} e^{-j\delta_{31}}\right] + n_2 \mathrm{Im}\left[\mathbf{C}_{32} e^{j(\delta_{21}-\delta_{31})}\right] + n_3 \mathrm{Im}\left[\mathbf{C}_{33}\right] + n_2^3 \mathrm{Im}\left[\mathbf{H}_3 e^{j(\delta_{21}-\delta_{31})}\right]. & \text{(25f)} \end{cases}$$

Note that the right hand sides of Eqs. (25) do not depend on θ_1 but on δ_{21} and δ_{31}.

Finally, combining Eqs. (25b) and (25d) as $(n_1(25\text{d}) - n_2(25\text{b}))/n_1 n_2$ and Eqs. (25b) and (25f) as $(n_1(25\text{f}) - n_3(25\text{b}))/n_1 n_3$ and grouping with Eqs. (25a), (25c) and (25e), we obtained the close form differential equations

$$\dot{\mathbf{\Lambda}} = \mathbf{F}\left(\mathbf{\Lambda}\right), \quad \text{with} \quad \mathbf{\Lambda} = \left[n_1 \; n_2 \; n_3 \;\; \delta_{21} \; \delta_{31}\right]^t. \tag{26}$$

Fixed points $\mathbf{\Lambda^e} = \left[n_1^e \; n_2^e \; n_3^e \;\; \delta_{21}^e \; \delta_{31}^e\right]^t$ of Eqs. (26) are computed by solving $\mathbf{F}\left(\mathbf{\Lambda^e}\right) = 0$ and associated stability property are found by looking the sign of the real parts of the eigenvalues λ_i (with $i \in [1, 5]$) of the Jacobian matrix of $\mathbf{F}$ evaluated at $\mathbf{\Lambda^e}$.

This analysis permits to predict the existence of stable periodic response regimes which correspond to the case where the real parts of all the eigenvalues are negative. In the following section, an asymptotic analysis of the complexified-averaged model is developed to characterize response regimes when stable property is not satisfied.

3.4 Asymptotic analysis of the complexified-averaged model

In this section we assume that $\epsilon \ll 1$ (i.e the mass of the NES is small with respect to the total mass of the fuselage and the blades) and that the parameters $\tilde{\lambda}_y, \tilde{\lambda}_\delta, \tilde{S}_d, \tilde{S}_c, \tilde{\mu}$ and $\tilde{\alpha}_3$ are of order ϵ (i.e $\tilde{\lambda}_y, \tilde{\lambda}_\delta, \tilde{S}_d, \tilde{S}_c, \tilde{\mu}, \tilde{\alpha}_3 \sim O(\epsilon)$). These parameters are rescaling as

$$\lambda_y = \frac{\tilde{\lambda}_y}{\epsilon}; \qquad S_d = \frac{\tilde{S}_d}{\epsilon}; \qquad \mu = \frac{\tilde{\mu}}{\epsilon}; \tag{27a}$$

$$\lambda_\delta; = \frac{\tilde{\lambda}_\delta}{\epsilon}; \qquad S_c = \frac{\tilde{S}_c}{\epsilon}; \qquad \alpha_3 = \frac{\tilde{\alpha}_3}{\epsilon}. \tag{27b}$$

with $\lambda_y, \lambda_\delta, S_d, S_c, \mu, \alpha_3 \sim O(1)$.

Moreover, we focus the analysis for Ω around $\omega_y + \omega_\delta$ introducing the detuning term a, defined as

$$\Omega = \omega_y + \omega_\delta + a\epsilon, \tag{28}$$

with $a \sim O(1)$.

Using the rescaled parameters, the terms $\mathbf{R}_{31}$, $\mathbf{L}_{31}$ and $\alpha_{r,1}$ can be expanded in a first-order Taylor series around $\epsilon = 0$ giving

$$\mathbf{R}_{31} = j + O\left(\epsilon^2\right) \tag{29}$$

$$\mathbf{L}_{31} = -\frac{\lambda_\delta}{8\omega_\delta}\epsilon + j\left(\frac{\omega_y + a\epsilon}{4\omega_\delta}\right) + O\left(\epsilon^2\right) \tag{30}$$

$$\alpha_{r,1} = -\frac{\lambda_\delta}{2}\epsilon + j\left(\omega_y + a\epsilon\right) + O\left(\epsilon^2\right). \tag{31}$$

Introducing Eqs. (29), (30) and (31) (neglecting the $O\left(\epsilon^2\right)$ terms) and the rescaled parameters (27), Eqs. (22) becomes

$$\begin{cases} \dot{\phi}_1 + \epsilon\left(\dfrac{\lambda_y + j\omega_y}{2}\phi_1 - j\dfrac{\omega_y}{2}\phi_2 - S_d\omega_y\phi_3\right) = 0 & \text{(32a)} \\ \dot{\phi}_2 + \dfrac{\epsilon\lambda_y}{2}\phi_1 - j\dfrac{\omega_y}{2}\left(\phi_1 - \phi_2\right)(1-\epsilon) - + \\ \qquad\qquad \epsilon S_d\omega_y\phi_3 + \phi_2(1+\epsilon)\left(\dfrac{\mu}{2} - j\dfrac{3\alpha_3}{8\omega_y^3}\left|\phi_2\right|^2\right) = 0 & \text{(32b)} \\ \dot{\phi}_3 + \epsilon\left(\left(\dfrac{\lambda_\delta}{2} - ja\right)\phi_3 - \dfrac{S_c\omega_y^2}{8\omega_\delta}\phi_1\right) = 0. & \text{(32c)} \end{cases}$$

Eqs. (32) define a simplified version of the complexified-averaged system which is called *full slow-flow system* which is now be analyzed using the multiple scale approach [17] with respect to the small parameter ϵ by considering *slow* time $t_0 = t$ and *super-slow* time[4] $t_1 = \epsilon t$. To achieve this, multiple scale expansion are introduced as

$$\phi_i = \phi_i(t_0, t_1) = n_i(t_0, t_1)e^{i\theta_i(t_0,t_1)} \text{ for } i = 1, 2, 3, \tag{33}$$

reported in Eqs. (32) with the derivative rule

$$\frac{d}{dt} = \frac{\partial}{\partial t_0} + \epsilon\frac{\partial}{\partial t_1}. \tag{34}$$

and finally isolating expressions of order ϵ^0 and ϵ^1 are deduced.

3.4.1 Slow time scale: ϵ^0-order of the system and Slow Invariant Manifold

The expressions of order ϵ^0 correspond to the following differential equations:

$$\begin{cases} \dfrac{\partial\phi_1}{\partial t_0} = 0 & \text{(35a)} \\ \dfrac{\partial\phi_2}{\partial t_0} = j\dfrac{\omega_y}{2}\left(\phi_1 - \phi_2\right) - \dfrac{\mu}{2}\phi_2 + j\dfrac{3\alpha_3}{8\omega_y^3}\phi_2\left|\phi_2\right|^2 & \text{(35b)} \\ \dfrac{\partial\phi_3}{\partial t_0} = 0. & \text{(35c)} \end{cases}$$

At the slow time scale, ϕ_3 is uncoupled with ϕ_1 and ϕ_2, and Eqs. (35a) and (35c) can be solved giving:

$$\begin{cases} \dfrac{\partial\phi_1}{\partial t_0} = 0 \implies \phi_1(t_0, t_1) = \Phi_1(t_1) & \text{(36a)} \\ \dfrac{\partial\phi_3}{\partial t_0} = 0 \implies \phi_3(t_0, t_1) = \Phi_3(t_1). & \text{(36b)} \end{cases}$$

Introducing the polar coordinates

$$\phi_j = n_j(t_0, t_1)e^{i\theta_j(t_0,t_1)} \text{ for } j = 1, 2 \text{ and } 3, \tag{37}$$

[4] We use the terminology introduced by Gendelman and Bar [6] whereby the term *fast* is reserved for the fast component $e^{j\omega_y t}$.

Eqs. (35) reduce to

$$\begin{cases} \dfrac{\partial n_1}{\partial t_0} = 0 & \text{(38a)} \\ \dfrac{\partial n_2}{\partial t_0} = \dfrac{\omega_y}{2}\left(n_1 \sin\delta_{21} + n_2 F_I(n_2)\right) & \text{(38b)} \\ \dfrac{\partial n_3}{\partial t_0} = 0 & \text{(38c)} \\ \dfrac{\partial \delta_{21}}{\partial t_0} = \dfrac{\omega_y}{2}\left(\dfrac{n_1}{n_2}\cos\delta_{21} - F_R(n_2)\right) & \text{(38d)} \\ \dfrac{\partial \delta_{31}}{\partial t_0} = 0, & \text{(38e)} \end{cases}$$

where (as in Section. (3.3)) the argument difference $\delta_{21} = \theta_2 - \theta_1$ and $\delta_{31} = \theta_3 - \theta_1$ have been introduced and the real scalar functions F_R and F_I are defined as

$$F(n_2) = F_R(n_2) + jF_I(n_2) = 1 - \frac{3\alpha_3}{4\omega_y^4}n_2^2 - j\frac{\mu}{\omega_y}. \tag{39}$$

The fixed points of Eq. (38) (which characterize the periodic solutions of Eqs. (19) at the slow time scale) can be computed directly by solving:

$$\lim_{t_0\to\infty}\frac{\partial n_2}{\partial t_0} = 0 \text{ and } \lim_{t_0\to\infty}\frac{\partial \delta_{21}}{\partial t_0} = 0. \tag{40}$$

Using Eq. (36a), Eqs. (38d) and (38c) reduce to the following form:

$$\Phi_1(t_1) = \Phi_2(t_1)F\left(|\Phi_2(t_1)|\right), \ \forall\Phi_3, \tag{41}$$

where

$$\lim_{t_0\to\infty}\phi_2(t_0,t_1) = \Phi_2(t_1). \tag{42}$$

It is interesting to note that Eq. (41) corresponds to the fixed point of Eq. (35b) i.e

$$\lim_{t_0\to\infty}\frac{\partial \phi_2}{\partial t_0} = 0.$$

As discussed for example in [20] for forced linear system with NES and in [7, 6] for nonlinear self-excitated system with NES, Eq. (41) defines the so-called *Slow Invariant Manifold* (SIM) but with respect to the variable (Φ_1, Φ_2, Φ_3).

Considering the polar coordinates

$$\Phi_j = N_j(t_1)e^{i\Theta_j(t_1)} \text{ for } j = 1, 2 \text{ and } 3, \tag{43}$$

it is convenient to characterize the SIM on the (N_1, N_2, N_3)-space as

$$N_1^2 = H(N_2) \tag{44}$$

where the real scalar function H is defined by

$$H(N_2) = N_2^2|F\left(N_2\right)|^2 = N_2^2\left[F_R(N_2)^2 + F_I(N_2)^2\right]. \tag{45}$$

The SIM does not depend on the variable N_3 and this structure can be analysed in the (N_2, N_1)-plan. The local extrema of the function $H(x)$ are given by the positive roots of its derivative H'. An easy calculus shows that the local extrema occur at

$$N_{2,M} = \frac{2}{3}\omega_y^2\sqrt{\frac{2-\sqrt{1-3\frac{\mu^2}{\omega_y^2}}}{\alpha_3}} \qquad N_{2,m} = \frac{2}{3}\omega_y^2\sqrt{\frac{2+\sqrt{1-3\frac{\mu^2}{\omega_y^2}}}{\alpha_3}} \tag{46}$$

if the following relation holds

$$\mu < \frac{1}{\sqrt{3}}\omega_y \tag{47}$$

and in this case $N_{2,M} < N_{2,m}$.

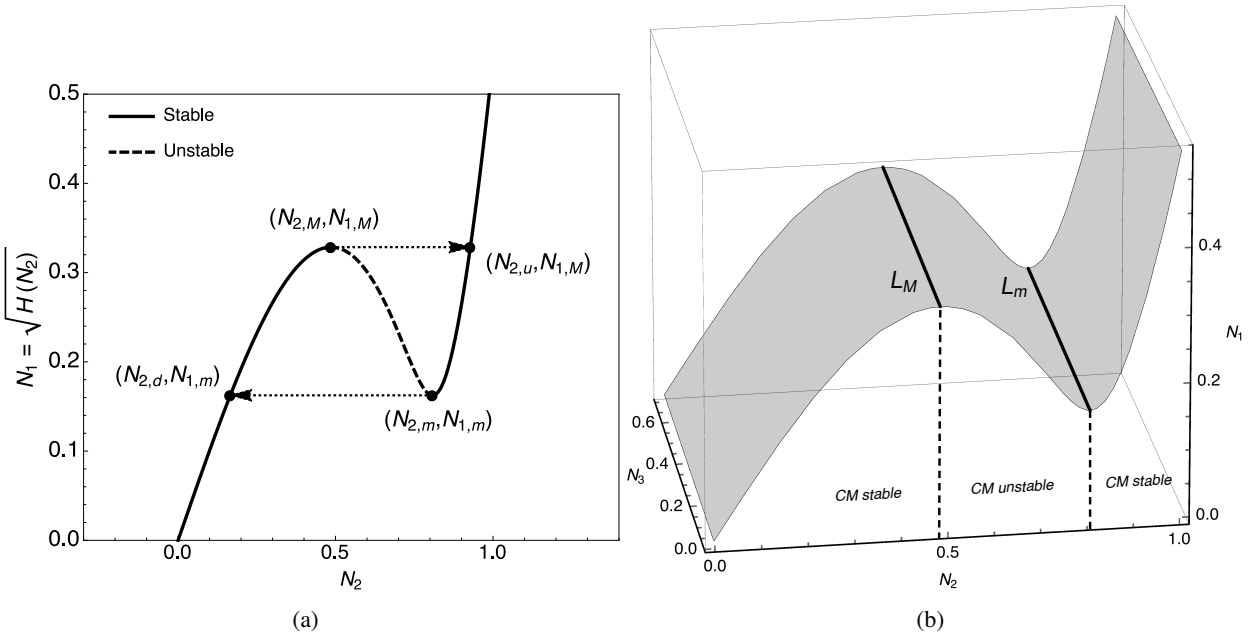

(a) (b)

Figure 4: *Slow Invariant Manifold* (SIM). Following parameters are used: $\omega_y = 1$, $\alpha_3 = 2$ and $\mu = 0.2$. (a) In the (N_1, N_2)-plan and (b) In the (N_1, N_2, N_3)-space.

Stability of the Slow Invariant Manifold. Stability range of the SIM is determined by examining the sign of the eigenvalues real parts of the Jacobian matrix of differential system (38b-38d) on the SIM. It can be shown that the condition of stability of the SIM is equivalent to:

$$H'(N_2) > 0 \tag{48}$$

and the stability range of the CM is characterized by the points $(N_{2,m}, N_{1,m})$ and $(N_{2,M}, N_{1,M})$ where $N_{1,M} = \sqrt{H(N_{2,M})}$, $N_{1,m} = \sqrt{H(N_{2,m})}$, which are therefore called *fold points* [19]. A typical *Slow Invariant Manifold* and it stability range are depicted (see Fig. 4(a)) in (N_2, N_1)-plan where $N_{2,d}$ and $N_{2,u}$ are solutions of

$$H(N_{2,m}) = H(N_{2,d}) \qquad \Rightarrow \qquad N_{2,d} = \frac{2\sqrt{2}}{3}\omega_y^2\sqrt{\frac{1-\sqrt{1-3\frac{\mu^2}{\omega_y^2}}}{\alpha_3}}, \tag{49}$$

and,

$$H(N_{2,M}) = H(N_{2,u}) \qquad \Rightarrow \qquad N_{2,u} = \frac{2\sqrt{2}}{3}\omega_y^2\sqrt{\frac{1+\sqrt{1-3\frac{\mu^2}{\omega_y^2}}}{\alpha_3}}, \tag{50}$$

respectively. In the (N_1, N_2, N_3)-space, each fold point defines a folded line (L_M and L_m) co-linear to the N_3-axis (see Fig. 4(b)).

The shape and the stability property of the SIM (i.e. the existence of folded lines on which the stability of the SIM changes) shown in Fig. 4 allow to define three steady-state regimes of the full slow-flow system (32) that can explain the three steady-state regimes of the SHM+NES described in Sect. 3.1.

A fixed point of the slow-flow is reached. These situations corresponds to a periodic solution of the SHM+NES (see Sects. 3.1 and 3.3).

Relaxation oscillations. The S-shape of the SIM suggests also the possible existence of *relaxation oscillations* [8]: starting at $S_0 \in L_M$, the system jumps to S_1, which is followed by a slow evolution of the

trajectory of the system (in the stable domain of the SIM) until it reaches L_m. After another jump and a slow evolution (in the stable domain of the SIM), the trajectory returns to $S_0 \in L_M$. Such scenario of relaxation oscillations for the slow-flow system can explain the existence of *Strongly Modulated Responses* [7, 6, 20] for the SHM+NES. Note that if $\mu > \omega_y/\sqrt{3}$, the S-shape nature of the SIM is lost and therefore relaxation oscillations are note possible.

Explosion. Until a first jump the slow-flow evolves the same way as for relaxation oscillations mechanism. However, instead of moving toward a stable fixed point or the folded line L_m, the trajectory of the system follows the SIM to the infinity. This scenario explains *no suppression* regime for the SHM+NES.

The existence of one of the three steady-state regimes described above or an other depends of the position and the stability of the fixed points of the full slow-flow system (32). Indeed, a stable fixed point of the full slow flow placed on the stable part of the SIM is a necessary condition to obtain PRs of the SHM+NES (17). On the other hand, the relaxation oscillations of the slow flow (or SRMs for the SHM+NES) can exist if both folded lines L_M and L_m have attractive parts. Position and stability of the fixed points of the full slow-flow system and attractivity (or repulsively) of the folded lines are determined in the next section through the study of the super-slow time scale.

3.4.2 Super-slow time scale: ϵ^1-order of the system

The expressions of order ϵ^1 correspond to the following differential equations:

$$\begin{cases} \dfrac{\partial \phi_1}{\partial t_1} = -\dfrac{\lambda_y}{2}\phi_1 - j\dfrac{\omega_y}{2}\left(\phi_1 - \phi_2\right) + S_d\omega_y\phi_3 & \text{(51a)} \\ \dfrac{\partial \phi_2}{\partial t_1} = -\dfrac{\lambda_y}{2}\phi_1 - j\dfrac{\omega_y}{2}\left(\phi_1 - \phi_2\right) + S_d\omega_y\phi_3 - \dfrac{\mu}{2}\phi_2 + j\dfrac{3\alpha_3}{8\omega_y^3}\phi_2\left|\phi_2\right|^2 & \text{(51b)} \\ \dfrac{\partial \phi_3}{\partial t_1} = -\left(\dfrac{\lambda_\delta}{2} - ja\right)\phi_3 + \dfrac{S_c\omega_y^2}{8\omega_\delta}\phi_1. & \text{(51c)} \end{cases}$$

We investigate the behavior of $\Phi_2(t_1)$ and $\Phi_3(t_1)$ with the super-slow time t_1. The behavior of $\Phi_1(t_1)$ is related to that of $\Phi_2(t_1)$ through the SIM (41)).

For this sake, we consider only Eqs. (51a) and (51c) in the limit $t_0 \to \infty$. Using Eqs (36a) and (42) and the SIM Eq. (41), Eqs. (51a) and (51c) are written as follow:

$$\begin{cases} \dfrac{\partial\left[\Phi_2 F(|\Phi_2|)\right]}{\partial t_1} = -\dfrac{\lambda_y}{2}\Phi_2 F(|\Phi_2|) - j\dfrac{\omega_y}{2}\Phi_2\left(F(|\Phi_2|) - 1\right) + S_d\omega_y\Phi_3 & \text{(52a)} \\ \dfrac{\partial \Phi_3}{\partial t_1} = -\left(\dfrac{\lambda_\delta}{2} - ja\right)\Phi_3 + \dfrac{S_c\omega_y^2}{8\omega_\delta}\Phi_2 F(|\Phi_2|). & \text{(52b)} \end{cases}$$

Introducing the polar coordinates

$$\Phi_2 = N_2(t_1)e^{i\Theta_2(t_1)} \text{ and } \Phi_3 = N_3(t_1)e^{i\Theta_3(t_1)}, \tag{53}$$

and separating real and imaginary parts, Eqs. (52) takes the following form:

$$\begin{cases} F_R\dfrac{\partial N_2}{\partial t_1} - N_2\dfrac{\partial \Theta_2}{\partial t_1}F_I + N_2\dfrac{\partial N_2}{\partial t_1}F_R' = -\dfrac{\lambda}{2}N_2F_R + \dfrac{\omega_y}{2}N_2F_I + S_d\omega_yN_3\cos\left(\Delta_{32}\right) & \text{(54a)} \\ N_2\dfrac{\partial \Theta_2}{\partial t_1}F_R + \dfrac{\partial N_2}{\partial t_1}F_I + N_2\dfrac{\partial N_2}{\partial t_1}F_I' = \\ \qquad\qquad -\dfrac{\lambda}{2}N_2F_I - \dfrac{\omega_y}{2}N_2\left(F_R - 1\right) + S_d\omega_yN_3\sin\left(\Delta_{32}\right) & \text{(54b)} \\ \dfrac{\partial N_3}{\partial t_1} = -\dfrac{\lambda}{2}N_3 + \dfrac{S_c\omega_y^2}{8\omega_\delta}N_2\big(F_R\cos\left(\Delta_{32}\right) + F_I\sin\left(\Delta_{32}\right)\big) & \text{(54c)} \\ \dfrac{\partial \Theta_3}{\partial t_1} = aN_3 + \dfrac{S_c\omega_y^2}{8\omega_\delta}N_2\big(F_I\cos\left(\Delta_{32}\right) - F_R\sin\left(\Delta_{32}\right)\big), & \text{(54d)} \end{cases}$$

involving the variable $\Delta_{32} = \Theta_3 - \Theta_2$. Combining Eqs (54a-54d), system of Eqs. (54) can be finally reduced (after some calculation steps) to the following form:

$$\begin{cases} H'(N_2)\dfrac{\partial N_2}{\partial t_1} = f_{N_2}\left(N_2, N_3, \Delta_{32}\right) & \text{(55a)} \\ H'(N_2)\dfrac{\partial \Delta_{32}}{\partial t_1} = f_{\Delta_{32}}\left(N_2, N_3, \Delta_{32}\right) & \text{(55b)} \\ \dfrac{\partial N_3}{\partial t_1} = f_{N_3}\left(N_2, N_3, \Delta_{32}\right), & \text{(55c)} \end{cases}$$

where

$$f_{N_2}\left(N_2, N_3, \Delta_{32}\right) = a_{11}\cos\Delta_{32} + a_{12}\sin\Delta_{32} - c_1, \quad (56)$$
$$f_{\Delta_{32}}\left(N_2, N_3, \Delta_{32}\right) = a_{21}\cos\Delta_{32} + a_{22}\sin\Delta_{32} - c_2, \quad (57)$$
$$f_{N_3}\left(N_2, N_3, \Delta_{32}\right) = a_{31}\cos\Delta_{32} + a_{32}\sin\Delta_{32} - c_3. \quad (58)$$

The coefficients a_{11}, a_{12}, a_{21}, a_{22}, a_{31}, a_{32}, c_1, c_2 and c_3 are not specified here. Eqs. (55) admit 0, 1 or 2 fixed points denoted $\{N_2^e, N_3^e, \Delta_{32}^e\}$ and defined by:

$$f_{N_2}\left(N_2^e, N_3^e, \Delta_{32}^e\right) = 0, \quad (59a)$$
$$f_{\Delta_{32}}\left(N_2^e, N_3^e, \Delta_{32}^e\right) = 0, \quad (59b)$$
$$f_{N_3}\left(N_2^e, N_3^e, \Delta_{32}^e\right) = 0 \quad (59c)$$
$$H'(N_2^e) \neq 0. \quad (59d)$$

If $\epsilon \ll 1$, fixed points computed from Eqs. (59) corresponds to fixed points of the system (26) obtained in Sect. 3.3. As usual, stability of the fixed points are found by looking the sign of the eigenvalues real parts of the Jacobian matrix of the vector function $\mathbf{F_1} = (f_{N_2}/g, f_{\Delta_{32}}/g, f_{N_3})$ evaluated at $\{N_2^e, N_3^e, \Delta_{32}^e\}$.

3.5 Prediction of the steady-state response regimes of the SHM+NES

The prediction of the steady-state response regimes of the SHM+NES (17) resulting from initial conditions not too far from the trivial equilibrium position is obtained checking first the local stability property of the trivial equilibrium point of Eqs. (17) (see Sect. 2.2.1) and using the asymptotic analysis of the full slow-flow system (32) to characterize the response regimes when the trivial equilibrium point of Eqs. (17) is unstable. From the asymptotic analysis of slow-flow system (32) performed in Sect. 3.4, we characterize

- the SIM (41) and its the fold points $N_{2,M}$ and $N_{2,m}$ (see Eqs. (46)) and the points $N_{2,d}$ and $N_{2,u}$ defined in Eqs (49) and (50) respectively,
- the stable periodic regimes (PRs) of Eqs. (17) as the stable fixed points of Eqs. (55),
- the non periodic response regimes (SMRs or no suppression) of Eqs. (17) from the unstable fixed points of Eqs. (55).

The steady-state response regimes are classified in five domains:

Domain 0 Complete suppression

Domain 1 Partial suppression through PR

Domain 2 Partial suppression through PR or SMR

Domain 3 Partial suppression through SMR

Example	a	μ	Number of Fixed Pt.	Fixed Pt. 1: $\{N_1^e, N_2^e, N_3^e\}$	Fixed Pt. 2: $\{N_1^e, N_2^e, N_3^e\}$
1a	-0.65	0.15	2	$\{0.312, 0.406, 0.211\}$ S	$\{0.448, 0.978, 0.412\}$ U
1b	0.3	0.7	1	$\{0.608, 0.859, 0.723\}$ S	–
2a	0.2	0.45	2	$\{0.372, 0.826, 0.539\}$ S	$\{151, 4.7, 75.4\}$ U
2b	0.2	0.37	1	$\{0.298, 0.799, 0.468\}$ S	$\{151, 4.7, 75.6\}$ U
3a	0.4	0.2	1	$\{0.195, 0.744, 0.319\}$ U	–
3b	-0.2	0.2	2	$\{0.239, 0.692, 0.307\}$ U	$\{1.22, 1.16, 0.77\}$ U
4a	0.65	0.3	2	$\{0.287, 0.870, 0.458\}$ U	$\{0.331, 0.593, 0.340\}$ U
4b	0.65	0.5	0	–	–

Table 1: Values of a and μ used in Examples 1a, 1b, 2a, 2b, 3a, 3b, 4a and 4b. Coordinates N_1^e, N_2^e and N_3^e of the corresponding fixed points of (55) are also indicated. S $\equiv$ stable and U $\equiv$ unstable.

Example	a	μ	$N_{2,M}$	$N_{2,m}$	$N_{2,u}$	$N_{2,d}$
1a	-0.65	0.15	0.479	0.812	0.935	0.124
1b	0.3	0.7	$\mu > \omega_y/\sqrt{3} \approx 0.577$			
2a	0.2	0.45	0.552	0.764	0.850	0.407
2b	0.2	0.37	0.523	0.784	0.886	0.321
3a	0.4	0.2	0.486	0.808	0.928	0.166
3b	-0.2	0.2	0.486	0.808	0.928	0.166
4a	0.65	0.3	0.505	0.796	0.908	0.254
4b	0.65	0.5	0.577	0.745	0.816	0.471

Table 2: Values of $N_{2,M}$, $N_{2,m}$, $N_{2,u}$ and $N_{2,d}$ corresponding to Examples 1a, 1b, 2a, 2b, 3a, 3b, 4a and 4b.

Domain 4 No suppresion

The diagram of the Fig. 5 summarizes the algorithm used to, for a given set of parameters, the corresponding domain for the associated response regime: Fig. 5(a) for $\mu < \omega_y/\sqrt{3}$ and Fig. 5(b) $\mu > \omega_y/\sqrt{3}$. The algorithm is detailed in the following section.

4 Parametric study and numerical validation of the prediction algorithm

The procedure presented in Sect. 3.5 is used to analyze the influence of the damping μ of the NES and the rotor speed Ω, through the detuning parameter a, on the response regimes of the SHM+NES model. The following set of numerical values of the parameters is used:

$$\begin{array}{llll} \omega_y = 1, & \omega_\delta = 2, & \lambda_y = 0.3, & \lambda_\delta = 0.15, \\ S_d = 1, & S_c = 2, & \alpha_3 = 2, & \epsilon = 0.01, \end{array} \tag{60}$$

with $\mu \in [0, 1]$ and $a \in [-1.2, 1.2]$. Results are plotted in Fig. 7 in which each domain is represented by an area of the plane (μ, a). Finally, for each domain (expect for Domain 0 which characterizes the *Complete suppression*) two examples are selected and studied deeply (see Figs. 8 to 13). The values of a and μ used for these examples and the corresponded coordinates N_1^e, N_2^e and N_3^e of the fixed points of (55) are indicated in Tab. 4. Tab. 2 shows the corresponded values of $N_{2,M}$, $N_{2,m}$, $N_{2,u}$ and $N_{2,d}$.

4.1 Domain 0: Complete suppression

Analytical prediction of the *complete suppression* is performed in Sect. 2.2.1. To obtain the Domain 0, the values of a that annul one of the eigenvalues Eqs. (17) are computed with respect to the parameter μ. For each value of μ, two values of a annul the eigenvalue, defining the functions $a^+(\mu)$ and $a^-(\mu)$ in the

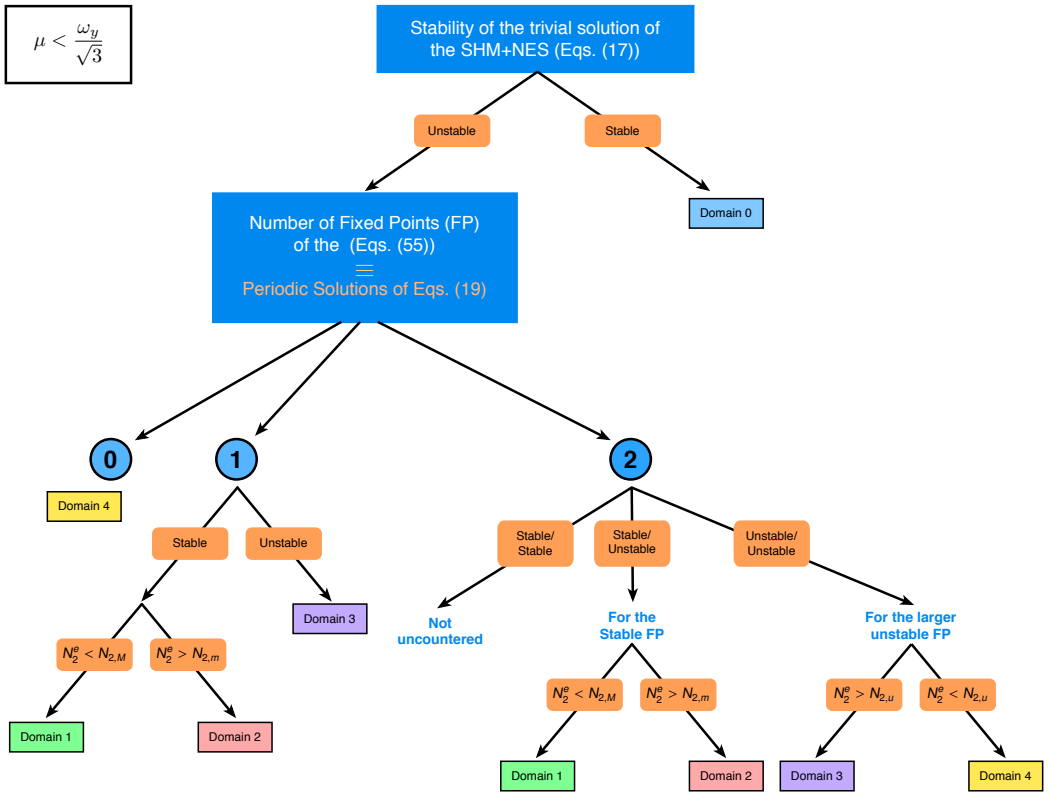

(a)

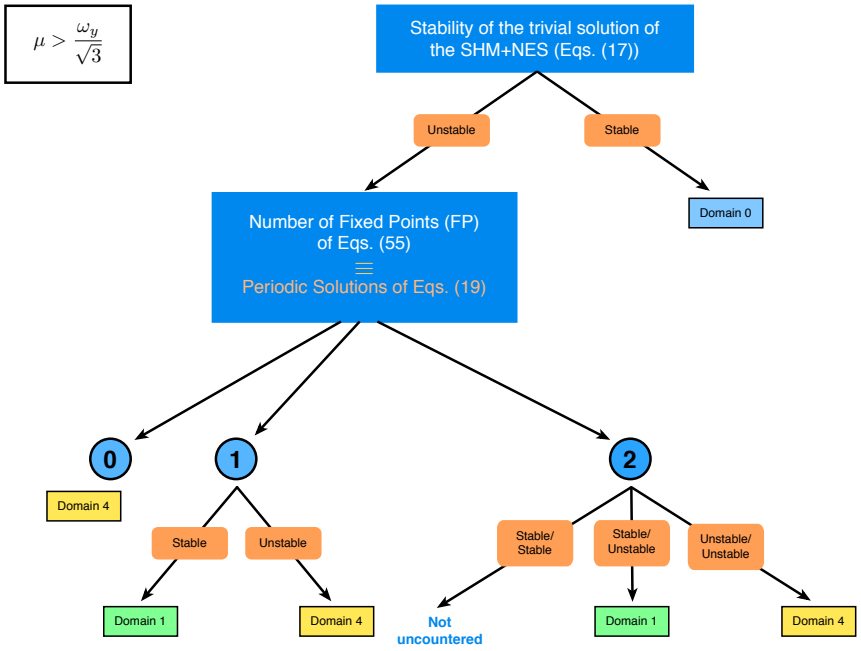

(b)

Figure 5: Algorithm for the determination of the domain of existence of the steady-state regimes of the SHM+NES (19). (a) $\mu < \omega_y/\sqrt{3}$ and (b) $\mu > \omega_y/\sqrt{3}$.

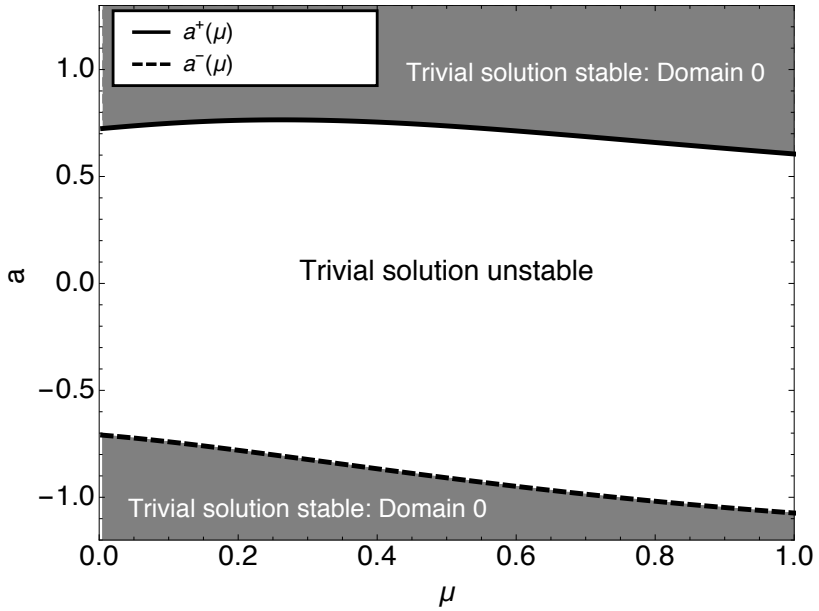

Figure 6: Functions $a^+(\mu)$ and $a^-(\mu)$ and Domain 0 which corresponds to the region of stability of the trivial solution of Eqs. (17). Parameters used: see Eq. (60).

plan (μ, a) (see Fig. 6). The area outside the curves $a^+(\mu)$ and $a^-(\mu)$ corresponds to stable trivial solution and in the area inside the curves, the trivial solution in unstable. The values $a^+(0)$ and $a^-(0)$ reflect the case without NES.

Remark. Following definitions correspond to situations for which $\mu < \omega_y/\sqrt{3}$. Otherwise, if $\mu > \omega_y/\sqrt{3}$, relaxation oscillations cannot exist. Therefore, only *Domains 1* and *Domains 4* are defined: *Domains 1* if one of the fixed point of slow-flow system is stable, *Domains 4* if not (see Fig. 5(b)).

4.2 Local stability of one of the fixed point of the slow-flow system: Domain 1 and 2

Fixed points of the slow-flow system correspond to periodic solutions of the SHM+NES. Therefore, the domain of existence the *Partial suppression through Periodic Response* may correspond to the domain of local stability of one of the fixed point. However, the two following situations must be considered: $N_2^e < N_{2,M}$ and $N_2^e > N_{2,m}$ where N_2^e is the N_2-coordinate of a stable fixed point. The two situations correspond to domain 1 and 2 respectively.

4.2.1 Domain 1: partial suppression through PR

This domain is represented by gray dots ("•") in Fig. 7. For $N_2^e < N_{2,M}$, the stable fixed point is reached before the folded line L_M. In this situation, relaxation oscillations or explosion of the slow-flow system and therefore SMR or *no suppression* regimes for the SHM+NES are avoided. Therefore, domain 1 corresponds to *Partial suppression through Periodic Response*. Figs. 8 and 9 show two examples of this situation with $\mu < \omega_y/\sqrt{3}$ and $\mu > \omega_y/\sqrt{3}$ respectively.

4.2.2 Domain 2: partial suppression through PR or SMR

This domain is represented by black crosses ("×") in Fig. 7. The case of one stable fixed point which satisfies the condition $N_2^e > N_{2,m}$ highlights the limit of the local stability study. Indeed, in this case, at least one jump from $N_{2,M}$ to $N_{2,u}$ is needed to reach the fixed point. After that, the fixed point can be really reached or sustained relaxation oscillations of the the slow-flow system are observed. Examples of the two possible situations are shown in Figs. 10 (PR, Example 2a) and 11 (SMR, Example 2b).

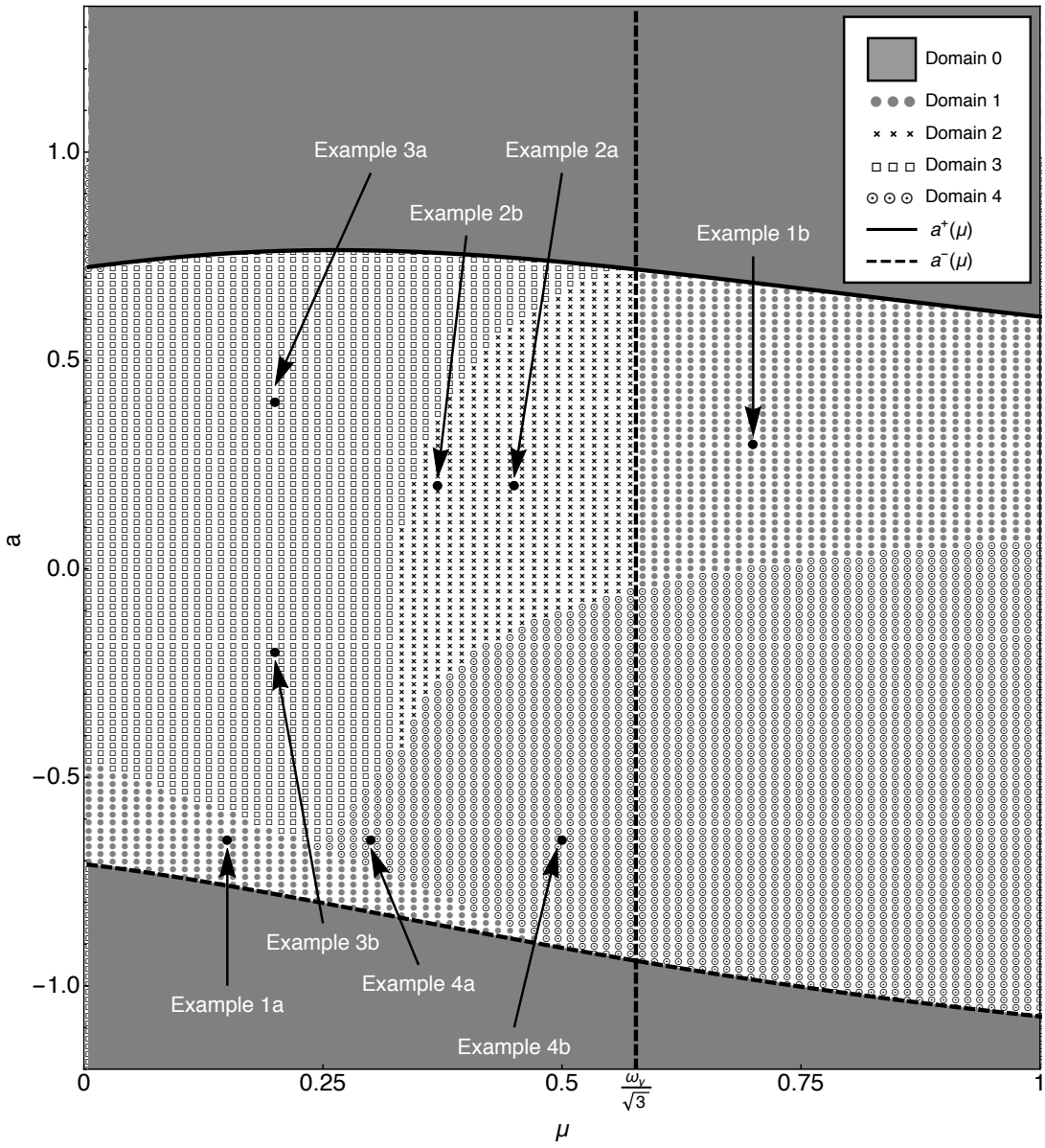

Figure 7: Prediction, in the plane (a, μ), of the domains of existence of the four steady-regimes. Domain 0: *Complete suppression* (the gray area). Domain 1: *Partial suppression through PR* (•). Domain 2: *Partial suppression through PR or SMR* (×). Domain 3: *Partial suppression through SMR* ("□"). Domain 4: *no suppression* ("⊙"). Parameters used: see Eq. (60).

4.3 Domain 3: partial suppression through SMR

This domain is represented by squares ("□") in Fig. 7 and corresponds to two situations. In the first situation, it exists one fixed point and it is unstable. In the second situation, there are two unstable fixed points and the larger of them should satisfied the following condition: $N_2^e > N_{2,u}$. Example 3a and Example 3b illustrate these two situations respectively (see Figs. 12 and 13). One can see in Figs. 12(b) and 13(b) that, in these situations, the fold points are reached by the system giving rise to relaxation oscillations of the slow-flow system which correspond to SMR for the SHM+NES.

4.4 Domain 4: no suppression

This domain is represented by dotted circles ("⊙") in Fig. 7 and corresponds to two situations. The first situation corresponds to the case of two unstable fixed points and for both fixed points we have: $N_{2,M} <$

$N_2^e < N_{2,u}$ (see Example 4a in Fig. 14). In the second situation, the slow-flow system has no fixed points. Therefore, there exists only the trivial solution of the SHM+NES, and it is unstable (see Example 4b in Fig. 15). In the case of *no suppression*, the GR instability is to strong to be suppressed by the NES attachment through PRs or SMRs and after a transient regime an explosion of the slow-flow in finally observed.

5 Conclusion

We studied the steady-state response regimes of a helicopter model reproducing GR instability coupled to ungrounded NES attached to the fuselage. A Simplest Helicopter Model (SHM) was defined as a linear system involving blade and fuselage dynamics resulting from Coleman and binormal transformations. This model reproduces the GR instability corresponding to frequency coalescence of the fuselage mode and the regressive rotor mode. The SHM is coupled to an ungrounded cubic NES defining the SHM+NES (Simplest Helicopter Model + Non Linear Energy Sink) model. To analyze the steady-state response regimes, the system is partitioned in slow-fast dynamics using complexification-averaging approach. The presence a small dimensionless parameter related to the mass of the NES in the slow-flow system implies that it involves one "slow" complex variable and two "super-slow" complex variables. The "super-slow/slow" nature of the system allowed us to use multiple scale approach to analyze it. In particular, the Slow Invariant Manifold of the slow flow was determined. Its shape involving two folded lines and the associated stability properties provide an analytical tool to explain and predict the existence of three regimes: periodic response regimes, strongly modulated response regimes and no suppression regimes that appear when the trivial solution is unstable. A procedure that allows determining the domains of existence of these regimes was proposed. This procedure was used to analyze the influence of the damping of the NES and the rotor speed on the response regimes of the SHM+NES model for a set of nominal numerical values of the other parameters of the model. In the unstable trivial solution area, four regimes were predicted: partial suppression through periodic response, partial suppression through strongly modulated response, partial suppression through periodic response or strongly modulated response and no suppression. All these regimes were validated from direct numerical integration of the SHM+NES model.

Acknowledgements

The authors wish to thank Mr. François Malburet for helpful discussions and suggestions. This research is done within the framework of the industrial chair "Dynamique des Systèmes Mécaniques Complexes (*Dynamics of complex mechanical systems*)" financed by the *Airbus Group Foundation*.

References

[1] R. Bellet, B. Cochelin, P. Herzog, and P.-O. Mattei. Experimental study of targeted energy transfer from an acoustic system to a nonlinear membrane absorber. *Journal of Sound and Vibration*, 329:2768–2791, 2010.

[2] A. R. S Bramwell, D Balmford, and G. T. S. Done. *Bramwell's helicopter dynamics*. 2001.

[3] T. K. Caughey and M. E. J. O'Kelly. *General theory of vibration of damped linear dynamic systems*. Dynamics Laboratory, California Institute of Technology, Pasadena, California, 1963.

[4] R. P. Coleman and A. M. Feingold. Theory of self excited mechanical oscillations of helicopter rotor with hinged blades. Technical report, NACA Report 1351, 1958.

[5] G. T. S. Done. A simplified approach to helicopter ground resonance. *Aeronautical Journal*, 78(761):204–208, 1974.

[6] O. V. Gendelman and T. Bar. Bifurcations of self-excitation regimes in a Van der Pol oscillator with a nonlinear energy sink. *Physica D*, 239(3-4):220–229, February 2010.

[7] O.V. Gendelman, A.F. Vakakis, L.A. Bergman, and D.M. McFarland. Asymptotic analysis of passive nonlinear suppression of aeroelastic instabilities of a rigid wing in subsonic flow. *SIAM Journal on Applied Mathematics*, 70(5):1655–1677, 2010.

[8] J. Grasman. *Asymptotic Methods for Relaxation Oscillations and Applications*, volume 63 of *Applied Mathematical Sciences*. Springer-Verlag, 1987.

[9] W. Johnson. *Helicopter theory*. Dover publications, inc., 1994.

[10] T. Krysinski and F. Malburet. *Instabilité mécanique: contrôle actif et passif*. Lavoisier, 2009.

[11] Y. S. Lee, A. F. Vakakis, L. A. Bergman, and D. M. McFarland. Suppression of limit cycle oscillations in the van der Pol oscillator by means of passive non-linear energy sinks. *Structural Control and Health Monitoring*, 13(1):41–75, January 2006.

[12] Y. S. Lee, A. F. Vakakis, L. A. Bergman, D. M. McFarland, and G. Kerschen. Suppression aeroelastic instability using broadband passive targeted energy transfers, part 1: Theory. *AIAA Journal*, 45(3):693–711, March 2007.

[13] Y. S. Lee, A. F. Vakakis, L. A. Bergman, D. M. McFarland, and G. Kerschen. Suppression aeroelastic instability using broadband passive targeted energy transfers, part 2: Experiments. *AIAA Journal*, 45(3):2391–2400, March 2007.

[14] A. W. Leissa. On a curve veering aberration (ZAMP). *Journal of Mathematics and Physics*, 25:99–111, 1974.

[15] A. Luongo and D. Zulli. Aeroelastic instability analysis of nes-controlled systems via a mixed multiple scale/harmonic balance method. *Journal of Vibration and Control*, 20(13):1985–1998, 2014.

[16] L.I. Manevitch. Complex representation of dynamics of coupled nonlinear oscillators. In LudmilaA. Uvarova, ArkadiiE. Arinstein, and AnatoliiV. Latyshev, editors, *Mathematical Models of Non-Linear Excitations, Transfer, Dynamics, and Control in Condensed Systems and Other Media*, pages 269–300. Springer US, 1999.

[17] A. H. Nayfeh. *Introduction to perturbation techniques*. Wiley VCH, 2011.

[18] L. Sanches, G. Michon, and D. Berlioz, A.and Alazard. Parametrically excited helicopter ground resonance dynamics with high blade asymmetries. *Journal of Sound and Vibration*, 331(16):3897–3913, 2012.

[19] R. Seydel. *Practical Bifurcation and Stability Analysis*, volume 5 of *Interdisciplinary Applied Mathematics*. Springer, 3ième edition, 2010.

[20] Y. Starosvetsky and O. V. Gendelman. Strongly modulated response in forced 2dof oscillatory system with essential mass and potential asymmetry. *Physica D*, 237(13):1719–1733, August 2008.

[21] A.F. Vakakis and O.V. Gendelman. Energy pumping in nonlinear mechanical oscillators: Part II - Resonance capture. *Journal of Applied Mechanics*, 68:42–48, 2001.

[22] A. F. Vakatis, O. V. Gendelman, L. A. Bergman, D. M. McFarland, G. Kerschen, and Y. S. Lee. *Nonlinear Targeted Energy Transfer in Mechanical and Structural Systems*. Springer-Verlag, Berlin, New York, 2008.

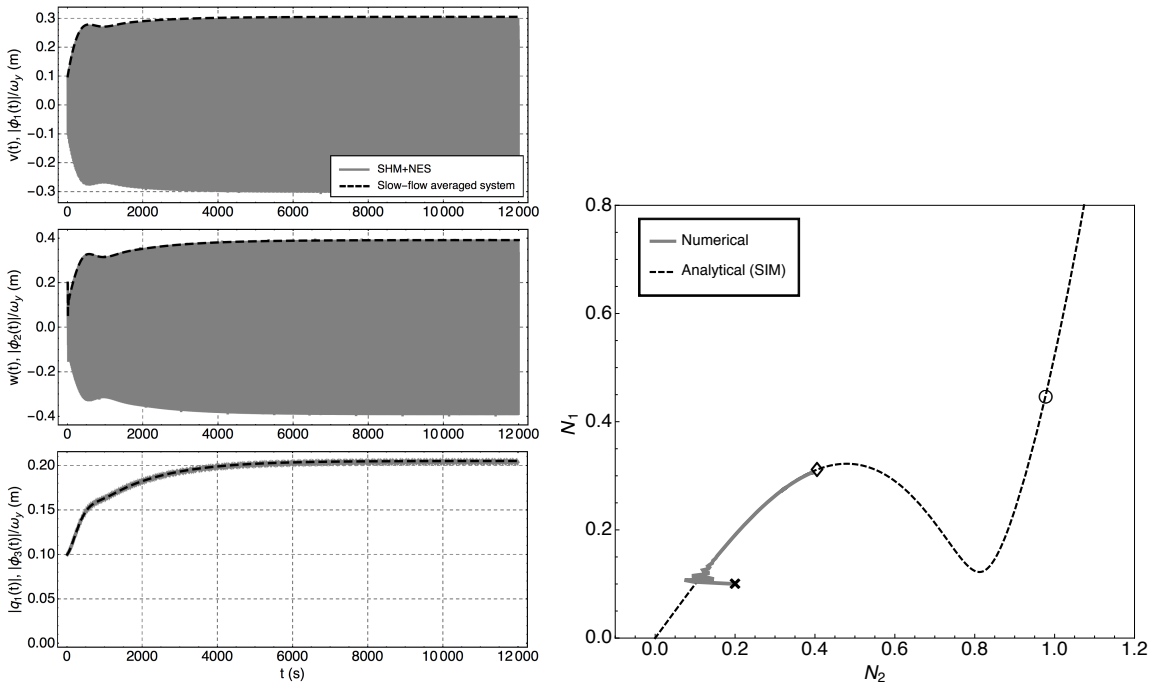

(a) (b)

Figure 8: Example 1. Parameters used: see Eq. (60), $a = -0.65$ and $\mu = 0.15$. (a) Comparison between numerical simulation of the SHM+NES (19) (gray solid line)) and the full slow-flow system (32) (black dashed line). (b) Comparison between the trajectory of the simulated slow-flow system (32) in the plane (N_2, N_1) and the *Slow Invariant Manifold* (41). "•": position $(N_{2,M}, N_{1,M})$, $(N_{2,m}, N_{1,m})$, $(N_{2,u}, N_{1,M})$ and $(N_{2,d}, N_{1,m})$, $\diamond$: stable fixed points, "$\circ$": unstable fixed points and $\times$: initial conditions.

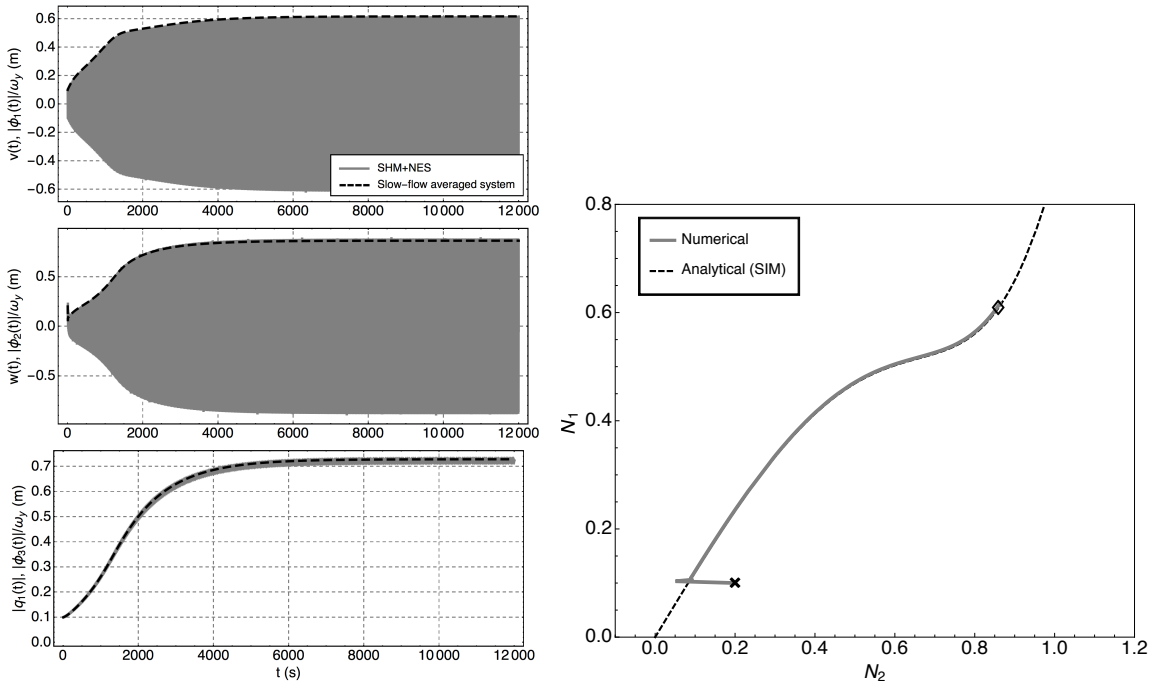

(a) (b)

Figure 9: Example 1b. Parameters used: see Eq. (60), $a = 0.3$ and $\mu = 0.7$. Same caption as for Fig. 8.

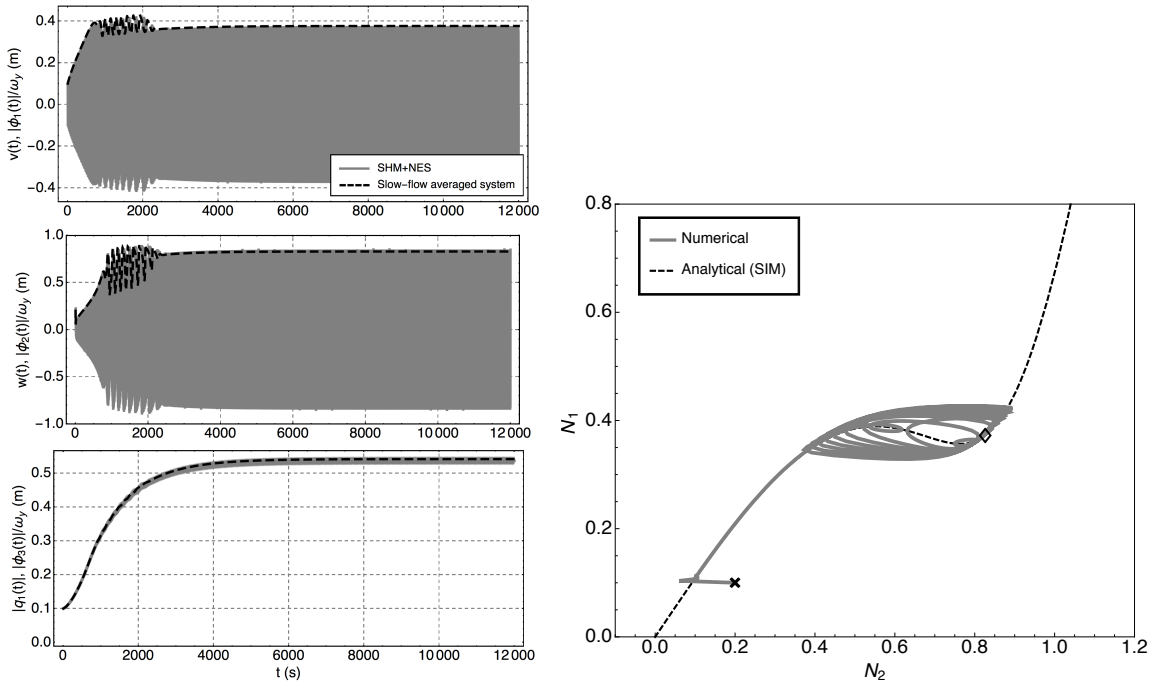

(a) (b)

Figure 10: Example 2a. Parameters used: see Eq. (60), $a = 0.2$ and $\mu = 0.45$. Same caption as for Fig. 8.

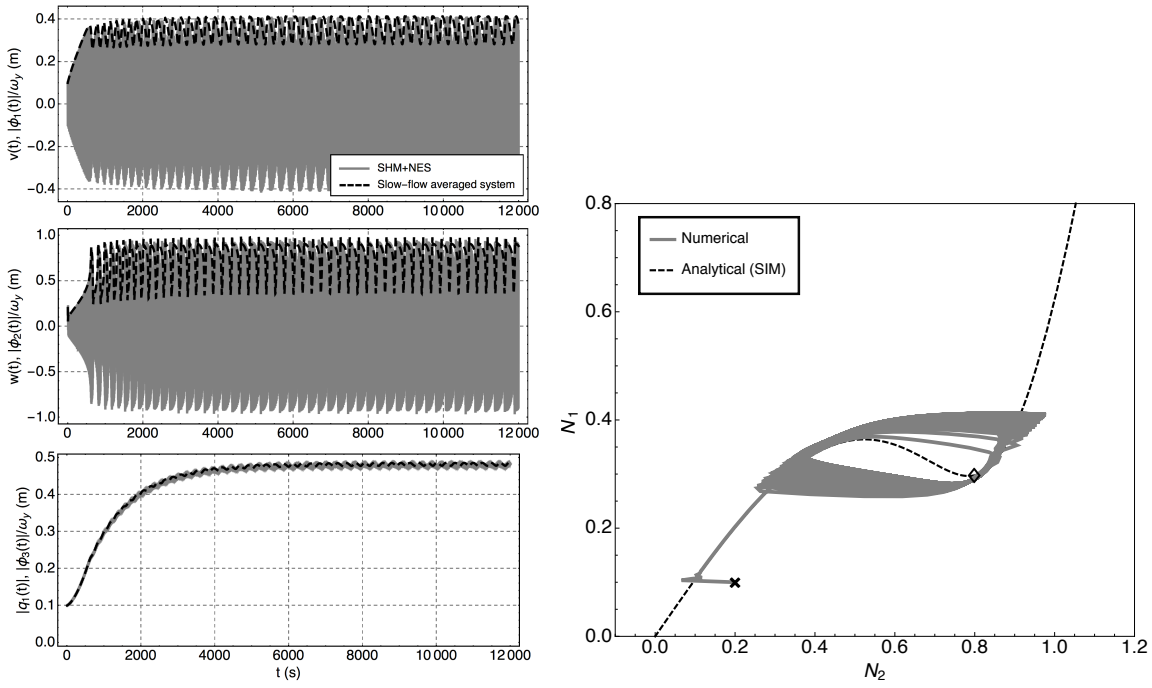

(a) (b)

Figure 11: Example 2b. Parameters used: see Eq. (60), $a = 0.2$ and $\mu = 0.37$. Same caption as for Fig. 8.

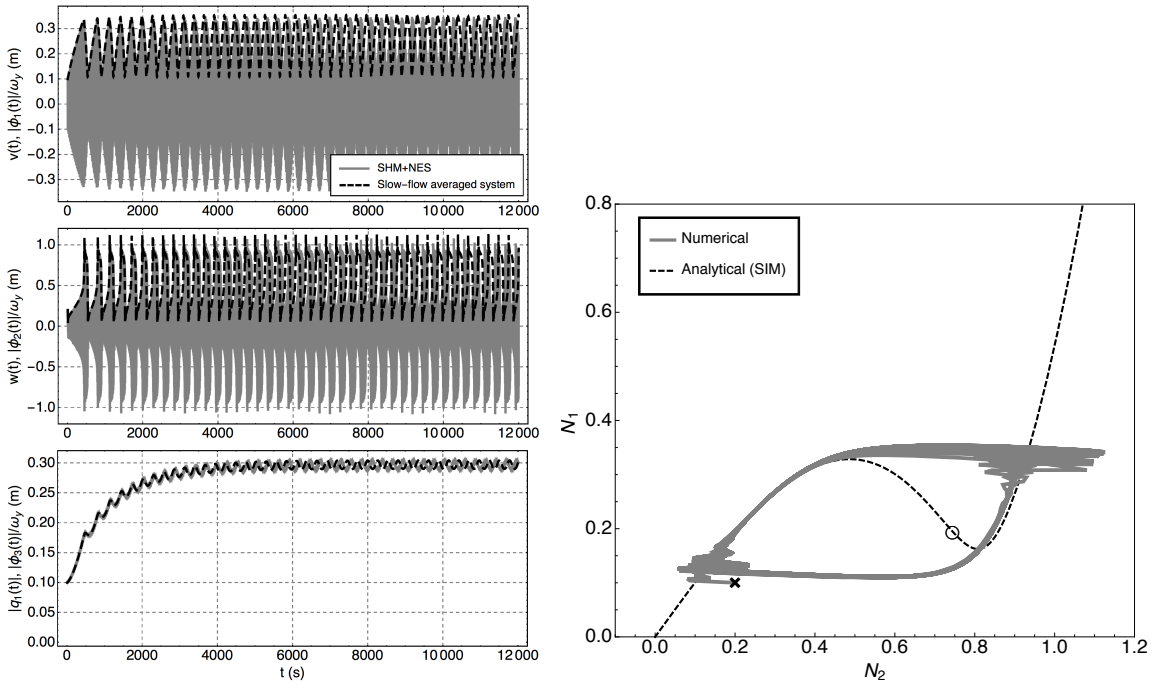

(a) (b)

Figure 12: Example 3a. Parameters used: see Eq. (60), $a = 0.4$ and $\mu = 0.2$. Same caption as for Fig. 8.

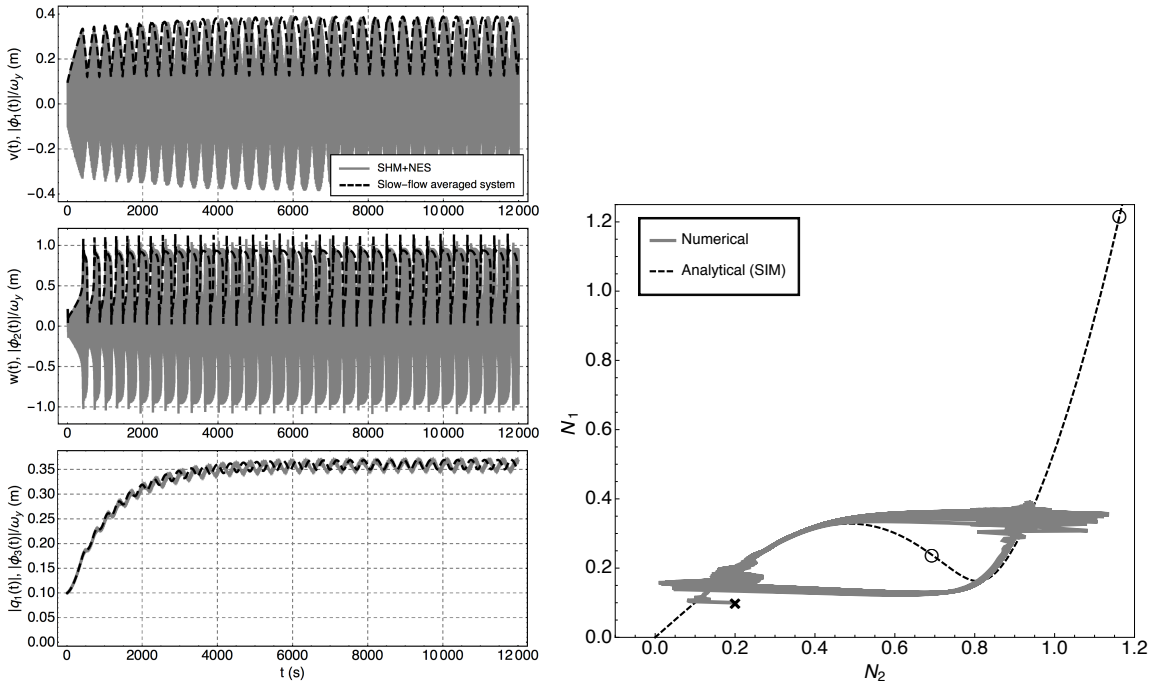

(a) (b)

Figure 13: Example 3b. Parameters used: see Eq. (60), $a = 0.2$ and $\mu = -0.2$. Same caption as for Fig. 8.

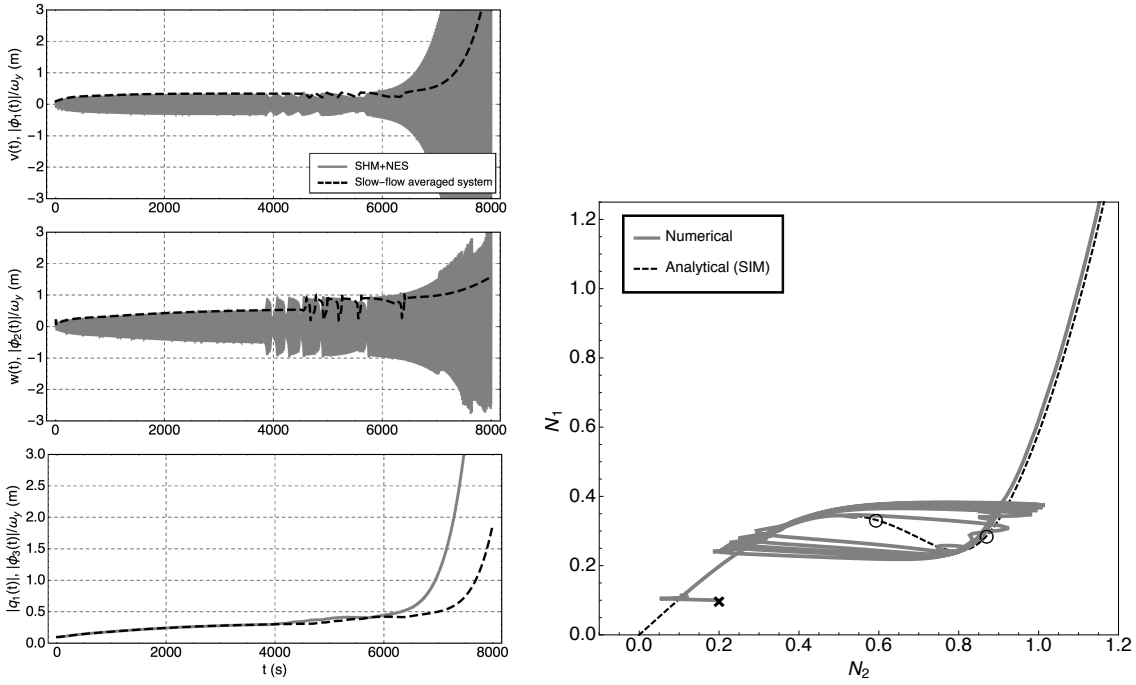

(a) (b)

Figure 14: Example 4a. Parameters used: see Eq. (60), $a = -0.65$ and $\mu = 0.3$. Same caption as for Fig. 8.

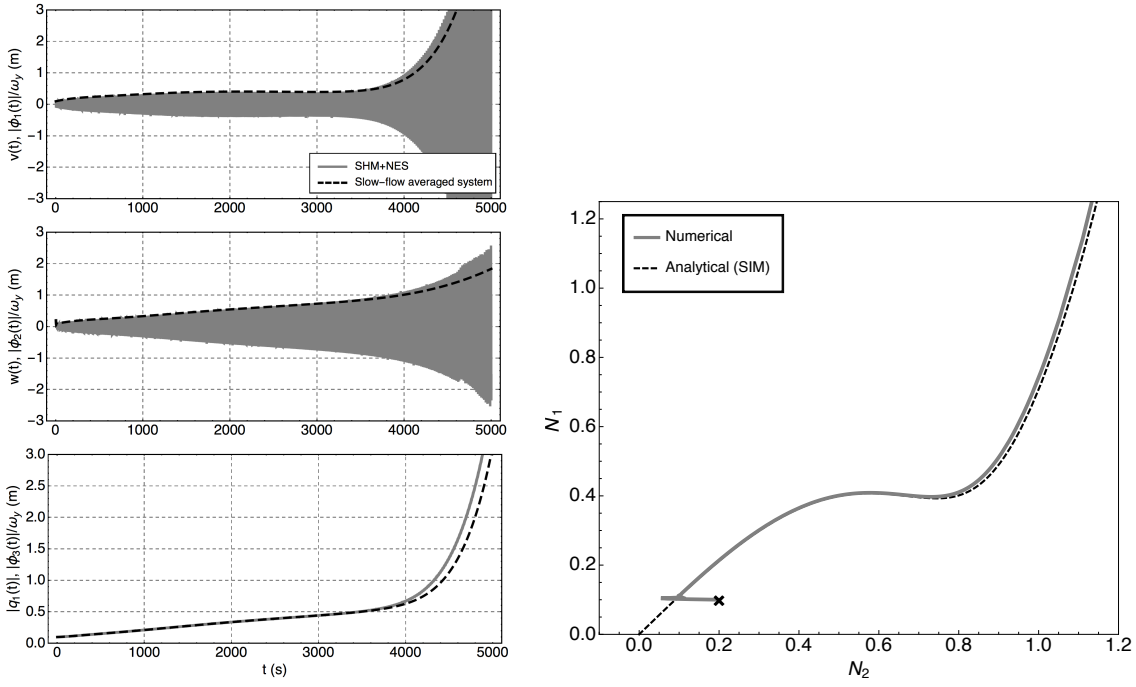

(a) (b)

Figure 15: Example 4b. Parameters used: see Eq. (60), $a = -0.65$ and $\mu = 0.5$. Same caption as for Fig. 8.